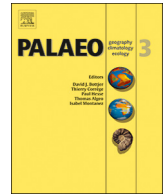




ELSEVIER

Contents lists available at ScienceDirect

Palaeogeography, Palaeoclimatology, Palaeoecology

journal homepage: www.elsevier.com/locate/palaeoTree-ring $\delta^2\text{H}$ values from lignin methoxyl groups indicate sensitivity to European-scale temperature changesT. Anhäuser^{a,b}, Birgit Sehls^a, Werner Thomas^c, Claudia Hartl^d, Markus Greule^a, Denis Scholz^e, Jan Esper^d, Frank Keppler^{a,f,*}^a Institute of Earth Sciences, Heidelberg University, Im Neuenheimer Feld 236, D-69120 Heidelberg, Germany^b Department of Chemical and Physical Sciences, University of Toronto Mississauga, Mississauga L5L 1C6, ON, Canada^c Deutscher Wetterdienst, Meteorological Observatory station Hohenpeißenberg, Albin-Schwaiger-Weg 10, 82383 Hohenpeißenberg, Germany^d Department of Geography, Johannes Gutenberg University Mainz, Johann-Joachim-Becher-Weg 21, 55128 Mainz, Germany^e Institute for Geosciences, Johannes Gutenberg University Mainz, Johann-Joachim-Becher-Weg 21, 55128 Mainz, Germany^f Heidelberg Center for the Environment HCE, Heidelberg University, D-69120 Heidelberg, Germany

ARTICLE INFO

Editor: H Howard Falcon-Lang

Keywords:

Stable hydrogen isotopes

Stable water isotopes

Paleoclimate proxy

Tree-ring archive

Temperature reconstruction

Moisture source

ABSTRACT

Stable hydrogen isotope ratios of lignin methoxyl groups ($\delta^2\text{H}_{\text{LM}}$) of wood have been shown to reflect climate-sensitive $\delta^2\text{H}$ values of precipitation ($\delta^2\text{H}_{\text{precip}}$). However, a detailed calibration study between high-resolution $\delta^2\text{H}_{\text{LM}}$ and $\delta^2\text{H}_{\text{precip}}$ data has not been performed yet. Here, we present annually resolved $\delta^2\text{H}_{\text{LM}}$ values from nine tree-ring series (derived from four *Fagus sylvatica* L. trees) collected near a station of the Global Isotope Network of Isotopes in Precipitation (GNIP) and the meteorological observatory at Hohenpeißenberg (Germany; $\sim 48^\circ\text{N}$, 11°E). The nine $\delta^2\text{H}_{\text{LM}}$ tree-ring series show highly significant inter-series correlations ($R_{\text{bar}} = 0.52$) over the common period of overlap 1916–2015 and no sign of a major juvenile trend affecting the first decades of growth. When compared with local instrumental data, the combined $\delta^2\text{H}_{\text{LM}}$ chronology is most indicative for annually averaged $\delta^2\text{H}_{\text{precip}}$ values. In line with this finding, the $\delta^2\text{H}_{\text{LM}}$ chronology shows similar climatic imprints as commonly observed for European stable water isotopes. We find the highest correlation ($r = 0.72$, $p < 0.001$) with temperature changes averaged over large-scale areas (range: 15°W – 20°E , 25 – 75°N) including marine and continental Western Europe. This large-scale temperature signal is not entirely stable over time, but weakens from 1948 to 1982 where 31-year running correlations drop systematically. The temporal signal strength coincides with a decline in R_{bar} values but also with known anomalous atmospheric circulation events (e.g., winter of 1956). We conclude two main findings. First, the temporal robustness of the transfer model is mainly controlled by the internal coherency among the tree-ring $\delta^2\text{H}_{\text{LM}}$ series. An improved understanding of such temporal discrepancies among the proxy data may therefore optimize reconstruction models. Second, this study highlights the need to critically assess the impact of changing atmospheric circulation patterns on the relationship between climate parameters and stable water isotopes.

1. Introduction

High-resolution tree-ring series are valuable climate archives fundamentally contributing to the understanding of past and current climate variability (Büntgen et al., 2011; Esper et al., 2019, 2002). Dendrochronological climate proxies are commonly used to reconstruct regional temperature variability derived, for instance, from tree-ring width (TRW) or maximum late wood density (MXD) from trees growing at or close to the altitudinal or latitudinal treeline (Esper et al., 2016; for hydroclimate see: Ljungqvist et al., 2020). Alternative proxies potentially suitable for climate reconstructions are tree-ring stable

hydrogen and oxygen isotope ratios (expressed as $\delta^2\text{H}$ and $\delta^{18}\text{O}$ values) since these partly reflect stable isotopes of the local precipitation ($\delta^2\text{H}_{\text{precip}}$ and $\delta^{18}\text{O}_{\text{precip}}$) (Augusti et al., 2008; Hartl-Meier et al., 2014; Hilasvuori et al., 2009; Liu et al., 2015; McCarroll and Loader, 2004; Pauly et al., 2018; Sternberg, 2009; Tang et al., 2000; Treydte et al., 2006; Voelker et al., 2014). Both $\delta^2\text{H}_{\text{precip}}$ and $\delta^{18}\text{O}_{\text{precip}}$ values are sensitive tracers of hydroclimate as they integrate a combination of (i) meteorological conditions in the moisture source area, (ii) changes during the meridional atmospheric vapor transport (particularly water volume loss, but also potential mixing of different air masses), and (iii) local temperature (Araguas-Araguas et al., 2000; Bowen et al., 2019;

* Corresponding author at: Institute of Earth Sciences, Heidelberg University, Im Neuenheimer Feld 236, D-69120 Heidelberg, Germany.

E-mail address: frank.keppler@geow.uni-heidelberg.de (F. Keppler).<https://doi.org/10.1016/j.palaeo.2020.109665>

Received 18 October 2019; Received in revised form 11 February 2020; Accepted 13 February 2020

Available online 19 February 2020

0031-0182/© 2020 Elsevier B.V. All rights reserved.

Dansgaard, 1964; Rozanski et al., 1993). Both stable water isotopes are therefore widely used proxies for a number of climate archives including ice cores, speleothems or lake sediments. Considering the global distribution of trees, suitable stable isotope proxies may therefore be particularly helpful in improving the spatial coverage of reconstructed stable water isotopes values. Furthermore, reconstructions of $\delta^2\text{H}_{\text{precip}}$ and $\delta^{18}\text{O}_{\text{precip}}$ values are able to complement commonly used tree-ring proxies (reflecting regional climate changes) with an additional stable isotope proxy (reflecting large-scale hydro-climatic changes).

When aiming to reconstruct stable water isotopes using tree-ring archives the compound of choice is commonly cellulose (e.g., Pauly et al., 2018; Treydte et al., 2006) since isotope signatures can differ among individual wood compounds (Cullen and Grierson, 2006; Wilson and Grinstead, 1977). However, cellulose incorporates hydrogen and oxygen atoms partly from leaf-water that experienced an evaporative ^2H and ^{18}O enrichment prior to biosynthesis (Anderson et al., 2002; Roden et al., 2000; Roden and Ehleringer, 1999; Sternberg, 2009; Voelker et al., 2014) potentially complicating the reconstruction of the initial source water $\delta^2\text{H}$ and $\delta^{18}\text{O}$ values. This has particularly been proven challenging for cellulose-derived $\delta^2\text{H}$ values as they are additionally controlled by plant physiological variability affecting internal fractionation processes (Augusti et al., 2008, 2006; Waterhouse et al., 2002). Moreover, to circumvent interferences with exchangeable hydrogen atoms, hydroxyl hydrogens must first be either replaced with nitro groups by nitration (DeNiro, 1981; Epstein et al., 1976; Yapp and Epstein, 1982) or equilibrated with water of known isotopic composition (Feng et al., 1993; Schimmelmann, 1991). The extraction procedures prior to stable hydrogen isotope analyses are therefore time consuming, particularly when aiming for a sufficient replication that allows statistical evaluation of the accompanied $\delta^2\text{H}$ and $\delta^{18}\text{O}$ variability among high resolution tree-ring series (McCarroll and Loader, 2004).

Another wood component that has been increasingly suggested for the investigation of $\delta^2\text{H}$ values in tree wood are lignin methoxyl groups (expressed as $\delta^2\text{H}_{\text{LM}}$ values; Anhäuser et al., 2017b, 2017a; Keppler et al., 2007; Riechelmann et al., 2017). Methoxyl groups (R-OCH₃) in wood are predominantly ether-bonded in lignin including hydrogen atoms that do not exchange with other hydrogen containing organic compounds or surrounding water. $\delta^2\text{H}_{\text{LM}}$ values of wood can therefore readily be measured as methyl iodide (CH₃I) upon treatment with hydroiodic acid providing, when compared to cellulose $\delta^2\text{H}$ analysis, a fast and straightforward extraction method (Greule et al., 2008). Lignin, formed within the xylem tissue, is mainly derived from three precursor compounds: p-coumaryl, coniferyl and sinapyl alcohol (Boerjan et al., 2003). Contrary to cellulose, lignin methoxyl groups are therefore not suggested to incorporate hydrogen atoms derived from leaf water. Support for this distinction is given by Gori et al. (2013) observing only a minor common variability ($r^2 = 0.24, 0.15$ and 0.38 with $n = 76, 149$ and 73 , respectively) between $\delta^2\text{H}$ values of cellulose and lignin methoxyl measured on identical tree-ring series. Thus, even though cellulose and lignin methoxyl groups share a common source of hydrogen atoms (soil water), subsequent biochemical pathways define cellulose-derived $\delta^{18}\text{O}$ and $\delta^2\text{H}$ values primarily as a proxy for leaf water stable isotopes (Anderson et al., 2002; Roden et al., 2000; Roden and Ehleringer, 1999; Sternberg, 2009; Voelker et al., 2014) and $\delta^2\text{H}_{\text{LM}}$ values as a proxy for xylem water $\delta^2\text{H}$ values (Feakins et al., 2013).

Earlier studies have mainly evaluated and quantified the spatial $\delta^2\text{H}_{\text{precip}}-\delta^2\text{H}_{\text{LM}}$ relationship using numerous sampling sites across continental to global-scale transects (Anhäuser et al., 2017b; Keppler et al., 2007). Therein, $\delta^2\text{H}_{\text{LM}}$ analysis was applied on homogenized tree-ring sections covering the most recently collected one or two decades. These studies suggested that $\delta^2\text{H}_{\text{LM}}$ values reflect $\delta^2\text{H}$ values of the tree's source water ($\delta^2\text{H}_{\text{sw}}$ values) as significant relationships between $\delta^2\text{H}_{\text{LM}}$ and mean annual $\delta^2\text{H}_{\text{precip}}$ values have been observed (implying that $\delta^2\text{H}_{\text{sw}}$ values reflect an annual integral of site-specific $\delta^2\text{H}_{\text{precip}}$

values). As $\delta^2\text{H}_{\text{sw}}$ values were not measured in most of these studies, the estimated isotope fractionation was calculated between $\delta^2\text{H}_{\text{precip}}$ and $\delta^2\text{H}_{\text{LM}}$ (commonly expressed as the apparent isotope fractionation ϵ_{app}). It was therefore suggested that ϵ_{app} reflects primarily the biosynthetic isotope fractionation (ϵ_{bio}) during lignin methoxyl biosynthesis. Calculations of ϵ_{app} showed a broad agreement among various coniferous and deciduous tree-species ($n = 13$) with ϵ_{app} values of $-213 \pm 17\%$ except for *Picea abies* (L.) H. Karst. ($-237 \pm 19\%$; Anhäuser et al., 2017a). Other studies investigated site-specific $\delta^2\text{H}_{\text{LM}}$ variability among tree species at single sites (Anhäuser et al., 2017a; Feakins et al., 2013) showing maximum differences of $\leq 28\%$ among five trees (within a circumference of 200 m). Hence, the accompanied variability of ϵ_{app} (in the range of ± 17 to 19%) was mainly assigned to inter-tree variability and defines the accuracy to reconstruct 'absolute' $\delta^2\text{H}_{\text{precip}}$ values using $\delta^2\text{H}_{\text{LM}}$ values. Reconstructions of 'absolute' $\delta^2\text{H}_{\text{precip}}$ values have therefore been considered suitable for wood samples covering anticipated large $\delta^2\text{H}_{\text{precip}}$ changes (exceeding the accompanied ϵ_{app} variability of ± 17 to 19%) as recently observed in deep-time Eocene fossil wood specimens (Anhäuser et al., 2018).

Anhäuser et al. (2017a) suggested that relative temporal $\delta^2\text{H}_{\text{LM}}$ changes, measured from multiple tree-ring series, may reflect relative temporal $\delta^2\text{H}_{\text{precip}}$ changes much more accurately since the characterized main noise of ϵ_{app} (inter-tree variability) is minimized (Anhäuser et al., 2017a). Earlier studies conducted preliminary investigations of inter-annually resolved $\delta^2\text{H}_{\text{LM}}$ tree-ring series (Gori et al., 2013; Mischel et al., 2015; Riechelmann et al., 2017). However, a detailed evaluation of the temporal $\delta^2\text{H}_{\text{LM}}-\delta^2\text{H}_{\text{precip}}$ relationship was not possible either due to lacking site-specific instrumental $\delta^2\text{H}_{\text{precip}}$ data (Gori et al., 2013; Mischel et al., 2015; Riechelmann et al., 2017) or potentially insufficient tree-ring series length of two decades (Mischel et al., 2015). To evaluate in detail the significance of $\delta^2\text{H}_{\text{LM}}$ to reflect $\delta^2\text{H}_{\text{precip}}$ at high resolution and its potential for climate reconstructions, this study investigates tree-ring $\delta^2\text{H}_{\text{LM}}$ variability in the vicinity (< 2 km) of a GNIP and DWD station located at Hohenpeißenberg (Germany). Nine cores from four *Fagus sylvatica* L. specimens were used to perform inter-annually resolved $\delta^2\text{H}_{\text{LM}}$ measurements with a common period of overlap 1916–2015. The data allowed also to assess the co-variance among radii and different trees and to evaluate potential non-climatic influences such as tree age. Subsequently, the $\delta^2\text{H}_{\text{LM}}$ tree-ring series were compared to site-specific $\delta^2\text{H}_{\text{precip}}$ reference data as well as local climate data. Moreover, this study evaluates, for the first time, the influence of large-scale temperature changes and atmospheric circulation modes, such as the North Atlantic Oscillation (NAO), on tree-ring $\delta^2\text{H}_{\text{LM}}$ values.

2. Study site and local climate

The study was conducted around the Hoher Peißenberg Mountain near the Hohenpeißenberg municipality in Germany ($47^\circ 48' \text{N}$, $11^\circ 01' \text{E}$; ~ 800 m.a.s.l.; Fig. 1). The site is located in the northern Alpine foothills consisting of molasse deposits (marlstones and calcareous gravels) and is further characterized by eutric cambisols, no permafrost and deciduous broadleaf forest.

Mean annual temperatures (MAT) during the 1916–2015 period ranged from 4.8 to 8.5 °C with a mean value of 6.6 °C and monthly temperatures varying between -1.4 °C (January) and 15.2 °C (July) (Fig. 2a, b). For the same time period, total annual precipitation ranged between 780 and 1570 mm with an average of 1160 mm, whereby half of the total annual precipitation falls between May and August. Precipitation in December, January and February falls primarily as snow. Monthly resolved $\delta^2\text{H}_{\text{precip}}$ data are available from 1971 to 2008 from the nearby GNIP station (Fig. 2c, d). Weighted mean annual $\delta^2\text{H}_{\text{precip}}$ values show an average value of -75% with a seasonal range from -107 (February) to -52% (August). Long-term climate trends of the 1916–2015 period at Hohenpeißenberg show that MATs increased significantly by 0.12 °C per decade ($r = 0.56$, $p < 0.001$, $n = 100$),

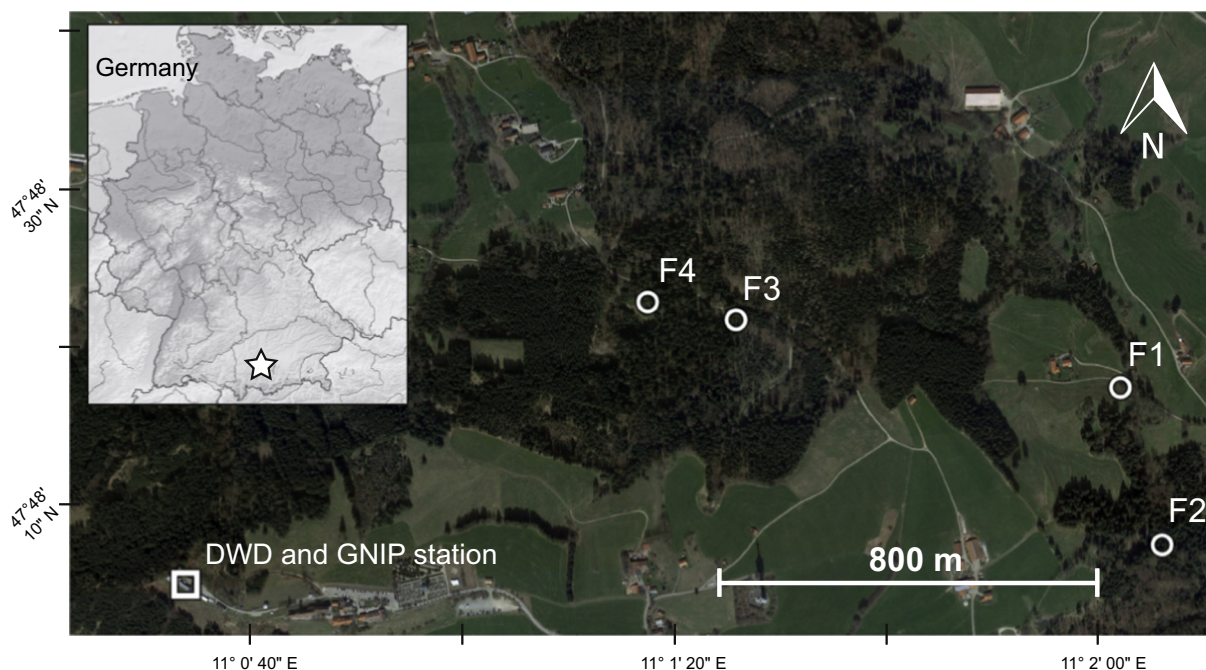


Fig. 1. Map of the investigation area. Top left shows the location of the sampling site Hohenpeißenberg (white star) in Germany. Circles in the areal picture mark the location of the four *Fagus sylvatica* L. specimens (F1-F4) used for tree ring $\delta^2\text{H}_{\text{LM}}$ measurements which are within a distance of 2 km from the German Weather Service (Deutsche Wetterdienst, DWD) and the Global Network of Isotopes in Precipitation (GNIP) station (square).

whereby neither significant changes in annual nor seasonal precipitation are observed (considering meteorological seasons). For the 1971–2008 period, weighted mean annual $\delta^2\text{H}_{\text{precip}}$ values correlate highly significantly with MAT ($r = 0.52, p < 0.001$), but show neither a significant correlation with annual ($r = -0.05, p = 0.62, n = 36$) nor with seasonal precipitation amount (r ranging from -0.32 to $0.20, p > 0.05$).

3. Material and methods

3.1. Tree-ring material

Twenty *Fagus sylvatica* trees were sampled in spring and autumn 2016. To assure maximum age coverage, individuals with large circumferences were chosen (2.0 to 4.5 m). We took two to three cores per

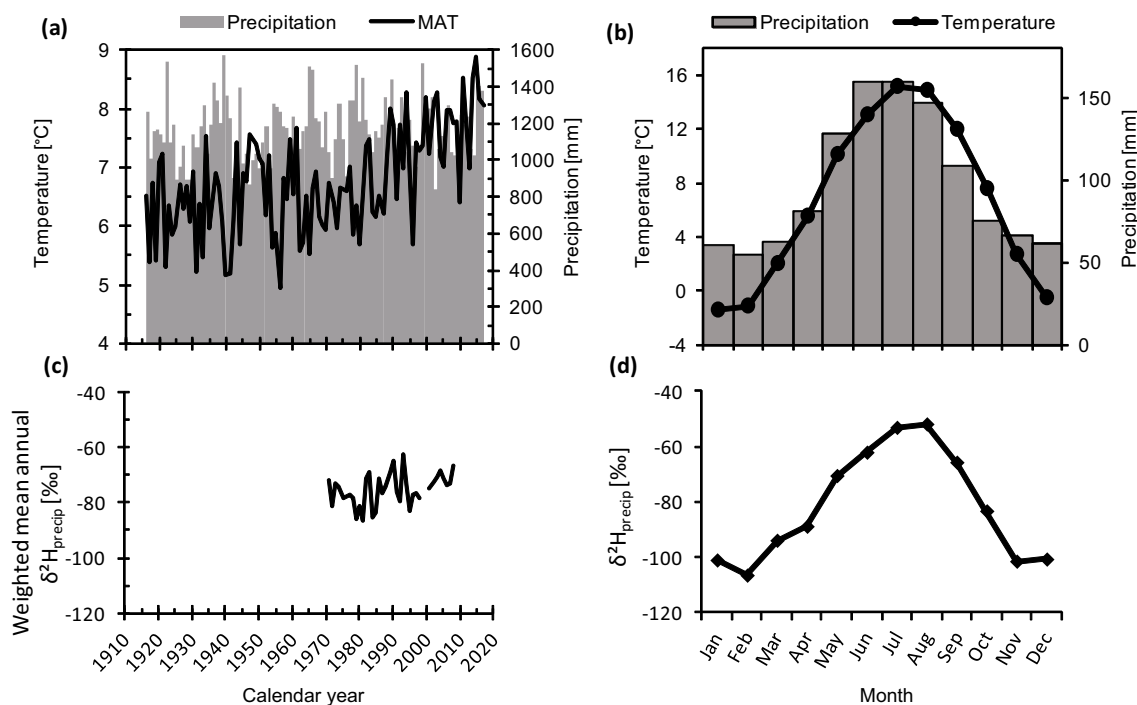


Fig. 2. Instrumental climate and $\delta^2\text{H}_{\text{precip}}$ data from the DWD and GNIP stations at Hohenpeißenberg. (a) Mean annual temperature (MAT) and total precipitation since 1916. (b) Seasonal temperature and precipitation patterns over the 1916–2015 period. (c) Weighted mean annual $\delta^2\text{H}_{\text{precip}}$ values for the 1971–2008 period (the years 1999 and 2000 are missing due to insufficient data). (d) Monthly resolved mean $\delta^2\text{H}_{\text{precip}}$ values for the 1971–2008 period.

Table 1
Sampling sites of the four *Fagus sylvatica* specimen and age coverage of the nine tree-rings series.

| Tree ID | Latitude; Longitude | Series ID | Pith offset | First year | Last year |
|---------|--------------------------------|-----------|-------------|------------|-----------|
| F1 | 47°48'17.50"N; 11°2'2.03"E | F1.1 | 7 | 1912 | 2015 |
| | | F1.2 | 0 | 1905 | 2015 |
| | | F1.3 | 7 | 1912 | 2015 |
| F2 | 47°48'7.57"N; 11°2'5.96"E | F2.1 | 23 | 1858 | 2015 |
| | | F2.2 | 8 | 1844 | 2015 |
| F3 | 47°48'21.78"N; 11°1'25.85"E | F3.1 | 7 | 1890 | 2015 |
| | | F3.2 | 33 | 1916 | 2015 |
| F4 | 47°48'22.90"N; 11°1'17.52"E | F4.1 | 6 | 1896 | 2015 |
| | | F4.2 | 26 | 1916 | 2015 |

tree at breast height (~1.2 m above ground) with a 5-mm increment borer yielding a total number of 52 cores (core lengths ranged from 400 to 600 mm). After collection, increment cores were cut perpendicular to the wood fibers using a core-microtome to ease ring identification (Gärtner and Nievergelt, 2010). Tree-ring width (TRW) was measured for all cores with an accuracy of 0.01 mm using a LINTAB measuring table equipped with TSAP-Win Software (both Rinntech, Heidelberg, Germany). Cross-dating accuracy was assessed visually and statistically using the program COFECHA (Holmes, 1983).

For δ^2H_{LM} analysis, four trees with no obvious disturbance influence, i.e., growth release or suppression, were selected (referred to as F1, F2, F3 and F4; cf. Fig. 1 and Table 1). To better assess intra-tree variability, we chose three cores of F1 and two cores of F2, F3 and F4 (termed F1.1, F1.2, F1.3 and so on). The four selected trees were either located at moderate east-facing slopes (< 10%), such as F1 and F2, or in flat terrain, such as F3 and F4. The longest tree-ring series of the four trees date back to 1905 (F1.2), 1844 (F2.2), 1890 (F3.1) and 1896 (F4.1) and were used to determine the 'pith offset' (number of missing innermost rings). The corresponding shortest tree-ring series for each tree dated back to 1912 (both F1.1 and F1.3), 1858 (F2.1), 1916 (F3.2) and 1916 (F4.2). Consequently, each tree provides a minimum of two radii that covered the 1916–2015 common period whereby two radii older than 1916 are provided by F2 (extending back to 1844 and 1858). Over the full periods, tree rings were carefully dissected at the tree ring border (latewood/earlywood transition) with a scalpel under a magnifier to subsequently allow annually resolved δ^2H_{LM} measurements. All dissected tree-ring samples yielded a minimum weight of 1 mg.

3.2. Instrumentation and analytical uncertainty of δ^2H_{LM} analysis

The δ^2H_{LM} value of wood can be measured as CH_3I released upon treatment of the samples with hydroiodic acid (HI) by the method described by Greule et al. (2008). Briefly, HI (0.25 ml; puriss. p.a., 55–60%, not stabilized, purchased from Sigma-Aldrich, Seelze, Germany, or Gillingham, UK, respectively) was added to the annually dissected tree-rings (1 to 10 mg, not homogenized) in a crimp glass vial (1.5 ml; IVA Analysentechnik, Meerbusch, Germany). The vials were sealed with crimp caps containing PTFE lined butyl rubber septa (thickness 0.9 mm) and incubated for 30 min at 130 °C. After heating, the samples were subsequently allowed to equilibrate at room temperature (22 ± 0.5 °C, air-conditioned room) for at least 30 min. Subsequently, an aliquot of the headspace (10–90 μ l) was collected and directly injected into the analytical system using an auto-sampler A200S (CTC Analytics, Zwingen, Switzerland) equipped with a gastight syringe (100 μ l, SGE Analytical Science).

The δ^2H values of the CH_3I formed from the methoxyl groups in the wood samples (δ^2H_{LM}) were measured using an HP 6890 N gas chromatograph (Agilent, Santa Clara, USA), coupled either to a Delta^{PLUS}XL isotope ratio mass spectrometer or to a 253 PlusTM isotope ratio mass spectrometer (both ThermoQuest Finnigan, Bremen, Germany) via a thermo conversion reactor (ceramic tube (Al_2O_3), length 320 mm,

0.5 mm i.d., reactor temperature 1450 °C) and a GC Combustion III Interface (ThermoQuest Finnigan, Bremen, Germany). The gas chromatograph (GC) was fitted with a Zebtron ZB-5MS capillary column (Phenomenex, Torrance, USA) (30 m \times 0.25 mm i.d., d_f 1 μ m), and the following conditions were employed: split injection (4:1), initial oven temperature at 30 °C for 3.8 min, ramp at 30 °C/min to 100 °C. Helium was used as carrier gas at a constant flow rate of 0.6 ml/min.

A tank of high purity hydrogen gas (H_2 , hydrogen 5.0, Linde, Höllriegelskreuth, Germany) with a δ^2H value ranging from -195 to -225‰ (vs. V-SMOW, range provided by the supplier) was used as the working reference gas. The H_3^+ factor, determined daily during the measurement period, was between 1.9 and 2.4 ppm/nA.

All δ^2H_{LM} values were normalized by a two-point linear calibration (Paul et al., 2007) using δ^2H values of two CH_3I working standards relative to V-SMOW. The δ^2H values of the CH_3I working standards were calibrated against international reference substances (VSMOW2 [$\delta^2H_{VSMOW} = 0.0 \pm 0.3\text{‰}$] and SLAP2 [$\delta^2H_{VSMOW} = -427.5 \pm 0.3\text{‰}$]) using an elemental analyser-isotopic ratio mass spectrometer (IsoLab, Max Planck Institute for Biogeochemistry, Jena, Germany). The calibrated δ^2H values in ‰ versus V-SMOW for the two CH_3I working standards were $-173.0 \pm 1.5\text{‰}$ ($n = 9, 1\sigma$) and $-66.2\text{‰} \pm 1.2\text{‰}$ ($n = 8, 1\sigma$). All samples were measured in triplicate followed by consecutive injections of both working standards. Standard deviations (1σ) of the triplicate measurements averaged $\pm 1.4\text{‰}$ (ranging from $< \pm 0.1$ to 13.9‰). Additional uncertainty is introduced by the 'external precision' (also referred as the chemical replication uncertainty). To estimate this uncertainty, we cut tree rings ($n = 68$) parallel to growth direction to obtain three tree-ring subsamples of the same cambial age (each comprising early and late wood). These subsamples enabled three separate HI treatments and subsequent δ^2H_{LM} analysis. The standard deviation of the three subsamples ($n = 68$) averaged $\pm 2.7\text{‰}$ (1σ) and was used as estimator for the 'external precision'. Using Gaussian error propagation, the overall analytical uncertainty of the δ^2H_{LM} determination averaged $\pm 3.6\text{‰}$ (ranging from ± 3.3 to $\pm 14.4\text{‰}$ with $n = 1086$).

3.3. δ^2H_{LM} covariance assessment and calibration

Coherency among the nine δ^2H_{LM} tree-ring series was assessed over the 1916–2015 common period using Pearson's correlation coefficient (r), inter-series correlation (Rbar) and expressed population signal (EPS; Wigley et al., 1984). Calculations of these metrics were performed using the 'dplR' library in R programming (Bunn, 2008). Rbar was further employed to assess the internal coherency over time by estimating Rbar over 31-year segments. Furthermore, to test whether some anomalous tree-ring δ^2H_{LM} series causes a drastic decrease in internal coherency, we estimated modified Rbar values by consecutively removing one of the nine radii. To visualize the long-term δ^2H_{LM} coherency of the four *F. sylvatica* trees, we calculated for each series the annual δ^2H_{LM} deviation to its mean value of the 1961–1990 period and averaged the resulting index δ^2H_{LM} series for each tree to produce four mean δ^2H_{LM} series. To identify potential non-climatic trends of δ^2H_{LM} values of juvenile tree-rings, we compared linear trends among differently old trees over a common time period. First year autocorrelation (Lag-1) has been calculated to determine the influence of the previous year on δ^2H_{LM} .

At humid sites, such as Hohenpeißenberg, soil water drawn during the tree's growth period rather reflects an accumulation of multiple precipitation events fallen during and prior the growth period potentially even including winter precipitation (Allen et al., 2019). To estimate the temporal integral of the source water for the *F. sylvatica* trees, we calculated Pearson's correlation coefficients between tree-ring δ^2H_{LM} and δ^2H_{precip} (GNIP) for the 1971–2008 period using a variety of monthly, seasonal and annual mean values. Moreover, we also included δ^2H_{precip} signatures of months of the preceding fall as well as 'shifted' annual values, such as previous September to current August. Whenever

$\delta^2\text{H}_{\text{precip}}$ values were averaged, individual $\delta^2\text{H}_{\text{precip}}$ values were weighted by precipitation amount to obtain representative mean values.

Correlation coefficients between $\delta^2\text{H}_{\text{LM}}$ tree-ring series and local climate parameters of Hohenpeißenberg were assessed for the common period of overlap (1916–2015) employing data of the nearby DWD station. To assess large-scale temperature influences on the Hohenpeißenberg tree-rings, spatial correlations between $\delta^2\text{H}_{\text{LM}}$ and the HadCRUT4.6 ensemble data (Morice et al., 2012) were conducted over the 1916–2015 period. Due to the prevailing westerlies across Europe, we focused on areas mainly west of Hohenpeißenberg (~48°N, 11°E). Thus, spatial correlations with land and sea surface temperature (CRU TS 4.01 and HadsST1, respectively) were conducted from North Africa to Scandinavia and from the Eastern North Atlantic to mid-Europe (range: 20–80°N and 30°W–20°E) employing the KNMI climate explorer at 1° x 1° resolution (Royal Netherlands Meteorological Institute; <http://climexp.knmi.nl>). The reconstruction skill for $\delta^2\text{H}_{\text{LM}}$ tree-ring series and climate parameters was assessed by the Durbin-Watson statistics (DW) testing for lag-1 autocorrelation in the linear model residuals. Further verification statistics included the reduction of error (RE; Briffa et al., 1988) as well as the coefficient of efficiency (CE; Cook, 1994). Positive scores of both RE and CE value indicate reconstruction skill of the model (Cook, 1994).

The NAO, defined as the normalized sea-level pressure difference between the Icelandic Low and the Azores High, reflects the strength of westerly airflow over Europe is therefore an important control on European weather and climate (Hurrell, 1995). Recent studies showed an influence of the NAO on European stable water isotopes, particularly during winter (Baldini et al., 2008; Deininger et al., 2016; Field, 2010). To assess the influence of the NAO we calculated Pearson's correlations between $\delta^2\text{H}_{\text{LM}}$ tree-ring series and a variety of monthly averaged NAO indices (Jones et al., 1997).

4. Results and discussion

4.1. Intra- and inter-tree variability of the $\delta^2\text{H}_{\text{LM}}$ series

For the common period of overlap (1916–2015), maximum and minimum $\delta^2\text{H}_{\text{LM}}$ values of the nine tree-ring series ranged from –243 to –224‰ and –295 to –270‰, respectively, yielding maximum $\delta^2\text{H}_{\text{LM}}$ differences within a core ranging between 41 and 66‰ (Table 2, cf. Supplemental Table S1 and Fig. S2). Mean $\delta^2\text{H}_{\text{LM}}$ values ranged from -250 ± 8 to -271 ± 11 ‰ (1 σ standard deviation), whereby the magnitude of this range results rather from $\delta^2\text{H}_{\text{LM}}$ differences among trees (up to $\Delta 21$ ‰) than radii (up to $\Delta 5$ ‰; cf. Table 2). Hence, in agreement with earlier findings (Anhäuser et al., 2017a; Riechelmann et al., 2017), $\delta^2\text{H}_{\text{LM}}$ values can differ regarding ‘absolute’ values particularly between trees by up to 21‰. Anhäuser et al. (2017b) suggested that about half of the inter-tree variability results from site-

specific $\delta^2\text{H}$ differences of the tree source water (i.e., $\delta^2\text{H}$ differences may already exist prior to water uptake), highlighting, however, that deviations in the biosynthetic isotope fractionation cannot be excluded.

Employing the full length of each of the nine tree-ring series, highly significant correlations ($p < 0.001$) can be noted among the $\delta^2\text{H}_{\text{LM}}$ series, whereby somewhat higher r values are observed within trees (ranging from 0.49 to 0.73) compared to inter-trees (ranging from 0.37 to 0.66; Table 3). For the 1916–2015 period, the EPS value equals 0.91 exceeding the commonly accepted threshold of ≥ 0.85 . Hence, even though $\delta^2\text{H}_{\text{LM}}$ values can differ regarding ‘absolute’ values particularly between trees by up to 21‰, the common variability indicates that these ‘absolute’ $\delta^2\text{H}_{\text{LM}}$ differences remain predominantly constant over time. Over the same period, the inter-series correlation (Rbar) yielded 0.52, whereby values for the 31-year segments indicate a systematic change in coherency over time (Fig. 3a). Rbar shows values of around 0.45 at the beginning of the chronology, followed by a gradual decrease to its lowest value (0.22; segment centered at 1961) and a subsequent gradual increase towards its highest value (0.65; segment centered at 1996). When calculating the modified Rbar values (consecutively removing one of the nine radii prior Rbar estimation), values ranged between 0.50 and 0.55 indicating no anomalous individual $\delta^2\text{H}_{\text{LM}}$ series among the nine radii.

Autocorrelation (Lag-1) is high and ranges between 0.40 and 0.78 indicating strong lag effects inherent to all $\delta^2\text{H}_{\text{LM}}$ series. These autocorrelations may reflect an autocorrelation adopted from the $\delta^2\text{H}_{\text{precip}}$ values. An equivalent autocorrelation for the $\delta^2\text{H}_{\text{precip}}$ over the 1971–2008 period cannot be observed ($r = 0.22$, $p > 0.1$). However, a lack of autocorrelation in the $\delta^2\text{H}_{\text{precip}}$ data may not indicate an equivalent lack of autocorrelation for $\delta^2\text{H}_{\text{sw}}$ values. Whereas $\delta^2\text{H}_{\text{precip}}$ values are individually measured of monthly collected precipitation, the source water $\delta^2\text{H}$ value reflects an integral of multiple precipitation events or even seasons reflecting a water body with a progressively changing $\delta^2\text{H}$ value. Thus, it seems reasonable to assume an autocorrelation inherent to $\delta^2\text{H}_{\text{sw}}$, which is transferred to the $\delta^2\text{H}_{\text{LM}}$ tree-ring series. Nonetheless, the autocorrelations observed for the $\delta^2\text{H}_{\text{LM}}$ tree-ring series may also point to some hydrogen ‘storage effect’ such as the incorporation of remobilized hydrogen during the lignin methoxyl groups biosynthesis.

When observing the mean $\delta^2\text{H}_{\text{LM}}$ series standardized for each tree (Fig. 3c), both the short-term (inter-annual) and long-term (multi-decadal) changes in $\delta^2\text{H}_{\text{LM}}$ values are comparable in magnitude with up to ~20‰. The long-term $\delta^2\text{H}_{\text{LM}}$ trends can broadly be grouped into four phases including (1) a decline of ~20‰ from 1858 to 1916 (covered only by F2), (2) a ~15‰ increase from 1916 to 1956 retained in all trees, (3) a decrease of ~10‰ until 1981, and (4) an increase by ~25‰ during the most recent decades. The most recent increase in $\delta^2\text{H}_{\text{LM}}$ values is most pronounced in F4.

Table 2

Descriptive statistics of the nine $\delta^2\text{H}_{\text{LM}}$ tree-ring series of the four *Fagus sylvatica* trees.

| Series ID | $\delta^2\text{H}_{\text{LM}}$ [‰ vs. VSMOW] over 1916–2015 | | | | |
|-------------------|-------------------------------------------------------------|---------|--------------------------|----------------------------|-------------------------|
| | Minimum | Maximum | Difference (Max. – Min.) | Mean with SD (1 σ) | Autocorrelation (Lag-1) |
| F1.1 | –294 | –243 | 51 | –269 \pm 11 | 0.645 |
| F1.2 | –288 | –243 | 45 | –266 \pm 10 | 0.515 |
| F1.3 ^a | –295 | –236 | 59 | –271 \pm 11 | 0.408 |
| F2.1 | –270 | –228 | 43 | –250 \pm 8 | 0.495 |
| F2.2 | –287 | –224 | 63 | –251 \pm 8 | 0.782 |
| F3.1 | –279 | –231 | 48 | –251 \pm 8 | 0.473 |
| F3.2 | –293 | –227 | 66 | –252 \pm 13 | 0.598 |
| F4.1 | –277 | –231 | 46 | –261 \pm 11 | 0.653 |
| F4.2 | –272 | –231 | 41 | –261 \pm 15 | 0.718 |

^a Nine years (1923–1931) are missing due to analytical problems.

Table 3

Pearson's r (with n) between the nine annually resolved δ^2H_{LM} tree-ring series (all statistically significant at $p < 0.001$). Color shading indicates r values between radii of the same tree.

| r n | F1.1 | F1.2 | F1.3 | F2.1 | F2.2 | F3.1 | F3.2 | F4.1 | F4.2 |
|------------|------|------|------|------|------|------|------|------|------|
| F1.1 | | 0.65 | 0.67 | 0.52 | 0.65 | 0.66 | 0.37 | 0.43 | 0.49 |
| F1.2 | 104 | | 0.69 | 0.49 | 0.61 | 0.63 | 0.59 | 0.55 | 0.59 |
| F1.3 | 95 | 95 | | 0.59 | 0.51 | 0.52 | 0.51 | 0.56 | 0.47 |
| F2.1 | 104 | 104 | 95 | | 0.49 | 0.40 | 0.40 | 0.42 | 0.37 |
| F2.2 | 104 | 104 | 95 | 158 | | 0.63 | 0.53 | 0.65 | 0.66 |
| F3.1 | 100 | 100 | 91 | 100 | 100 | | 0.59 | 0.51 | 0.54 |
| F3.2 | 100 | 100 | 91 | 100 | 100 | 100 | | 0.56 | 0.59 |
| F4.1 | 100 | 100 | 91 | 100 | 100 | 100 | 100 | | 0.73 |
| F4.2 | 100 | 100 | 91 | 100 | 100 | 100 | 100 | 100 | |

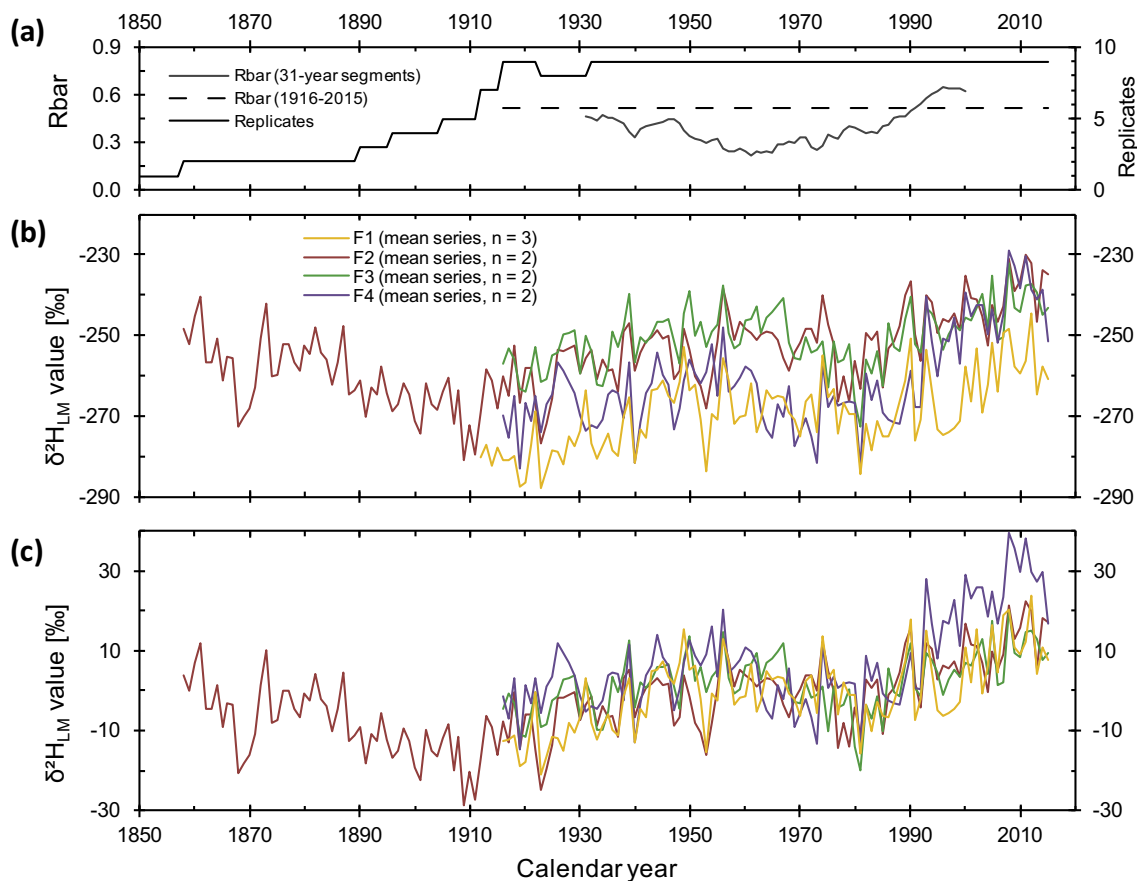


Fig. 3. Characteristics of the δ^2H_{LM} tree-ring series. (a) Rbar statistics for 31-year segments (black solid line) and for the full 1916–2015 period (dashed line) (b) Annually resolved δ^2H_{LM} values of the four *F. sylvatica* trees (F1, F2, F3 and F4) collected at Hohenpeißenberg (Germany). Each series reflects the mean δ^2H_{LM} series with $n = 2$ or 3. (c) Standardized tree-ring series of (b) using the mean δ^2H_{LM} value of the reference period 1961–1990.

Table 4

Statistics of the linear regression analysis of the four mean $\delta^2\text{H}_{\text{LM}}$ tree-ring series over the period 1916–1956 (as shown in Fig. 4). Series are ordered in accordance to reflected growth phase.

| Series | r ($p < 0.05$) | Slope with 95% CI [%/year] | Cambial age covered |
|--------|--------------------|----------------------------|----------------------|
| F2 | 0.39 | 0.24 ± 0.18 | 81–121 (mature) |
| F3 | 0.63 | 0.34 ± 0.14 | 34–74 (intermediate) |
| F4 | 0.50 | 0.31 ± 0.17 | 27–67 (intermediate) |
| F1 | 0.67 | 0.49 ± 0.18 | 12–52 (juvenile) |

4.2. Assessment of tree age related influences on $\delta^2\text{H}_{\text{LM}}$ values and mean chronology development

For cellulose-derived stable isotopes, non-climatic influences related to age have been observed over century-scale time periods (Esper et al., 2010; Treydte et al., 2006) as well as over the first three to four decades affecting rather juvenile tree-rings (Labuhn et al., 2014; Szymczak et al., 2012). Based on the length of our $\delta^2\text{H}_{\text{LM}}$ chronology of 100 years, we were able to evaluate the latter non-climatic influence commonly termed as ‘juvenile effect’. To test for this, we compared linear fits among the four mean $\delta^2\text{H}_{\text{LM}}$ series using the 1916–1956 period (above described as phase two) as here each series shows a significant positive linear trend sharing also a common positive $\delta^2\text{H}_{\text{LM}}$ excursion at the end of the period (1956; Fig. 3c). Moreover, during this 51-year period, the four *F. sylvatica* trees reflect different age phases including a juvenile phase of F1 (cambial age 12–52), intermediate phases of F4 and F3 (cambial age 27–67 and 34–74, respectively) as well as a mature phase of F2 (cambial age 81–121). This allows a statistical assessment of differences among $\delta^2\text{H}_{\text{LM}}$ trends and tree age (cf. Table 4). The slopes of the linear regressions over the period 1916–1956 become steeper with decreasing tree age phase (0.24 ± 0.18 , 0.34 ± 0.14 , 0.31 ± 0.17 and $0.49 \pm 0.18\%$ per year; Table 4; Fig. 4). However, when conducting a two-tailed *t*-test for slope differences, only the linear fits of juvenile F1 data and the mature F2 data are statistically different at $p < 0.1$. Hence, the elevated slope of F1 compared to F2 suggests a juvenile effect of F1 associated with increasing $\delta^2\text{H}_{\text{LM}}$ values (the slope difference between F1 and F2 equals 0.25% per year). Even though statistically significant, the magnitude of this potential ‘juvenile trend’ falls notably below the inter-annual $\delta^2\text{H}_{\text{LM}}$ variability of up to 20‰ (Fig. 3) as well as the average analytical overall uncertainty of $\pm 3.6\%$

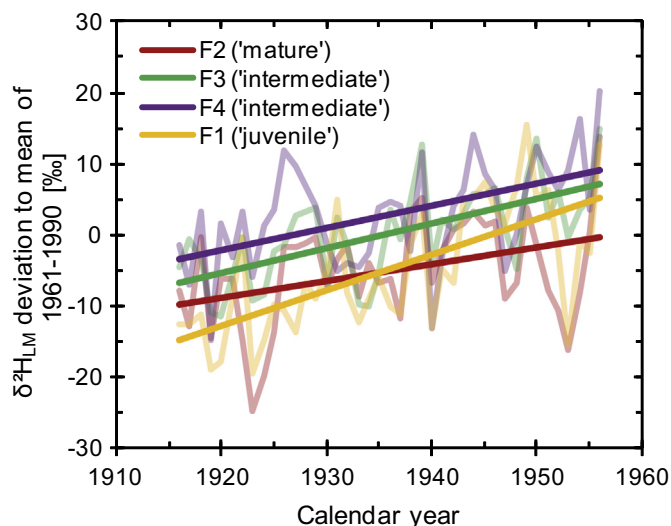


Fig. 4. Linear regression analysis of the four mean $\delta^2\text{H}_{\text{LM}}$ tree-ring series over the period 1916–1956. During this period, trees differ in age. Statistics of linear fits are given in Table 4.

and, thus, should have a negligible effect on the general coherency.

For cellulose-derived $\delta^2\text{H}$ and $\delta^{18}\text{O}$ tree-ring series, there are commonly two mechanisms considered to induce juvenile trends. First, arid study sites with high evaporation rates may lead to an evaporative enrichment of heavier stable isotopes in source waters of upper soil layers (Allison, 1982; Hsieh et al., 1998; Kanner et al., 2014). In presence of such a gradient in stable water isotopes in soils, trees would use consecutively less ^2H enriched soil waters over time as their root system progressively accesses deeper soil layers. Such a process would add a decreasing component to tree-ring $\delta^2\text{H}$ and $\delta^{18}\text{O}$ values until the root system is fully developed as has been suggested for a cellulose-derived $\delta^{18}\text{O}$ series from the Mediterranean region (Corsica, France; Szymczak et al., 2012). Another mechanism for juvenile trends may be induced by a gradient of relative humidity under the forest canopy. A decrease in relative humidity with height has been observed in temperate forests (Eliáš et al., 1989; Zweifel et al., 2002), which would intensify ^{18}O enrichment as leaf water evaporation rates increase with tree height (Labuhn et al., 2014). Hence, with increasing tree height (or age), leaf water would become gradually more enriched in heavy stable water isotopes. Contrary to the first mechanism, such a process would lead to increasing $\delta^2\text{H}$ and $\delta^{18}\text{O}$ values in juvenile tree-rings. However, for $\delta^2\text{H}_{\text{LM}}$ values, we consider only the first mechanism (soil water-related) as influential because leaf water-derived hydrogen is not involved in lignin methoxyl group's biosynthesis (Boerjan et al., 2003). Thus, as the juvenile $\delta^2\text{H}_{\text{LM}}$ values of F1 presented in this study show a minor mean trend deviation (associated with increasing $\delta^2\text{H}$ values), this indicates no impact of soil water-related juvenile effects, which would be associated with decreasing $\delta^2\text{H}$ values. This may either point to a weak or nonexistent gradient of soil water $\delta^2\text{H}$ values at Hohenpeißenberg or to a quickly developed root system of *F. sylvatica* trees within the first decade of growth. Nonetheless, future studies should take into account the potential influence of soil water evaporation rates on juvenile $\delta^2\text{H}_{\text{LM}}$ values, in particular for more arid study sites than Hohenpeißenberg.

A visibly stronger discrepancy in $\delta^2\text{H}_{\text{LM}}$ trends among the different trees can be observed for F4 at the end of our chronology (Fig. 3c). Comparing this discrepancy to F3, having a similar age as F4 (7 years apart; Table 1), suggests an influence not related to tree age. Similar conclusions can be drawn considering the moving Rbar values (Fig. 3a). The indicated coherency decrease occurs in the central part of our chronology, which only partly overlaps with the juvenile phase of F1. Consequently, deviations in the temporal $\delta^2\text{H}_{\text{LM}}$ trends seem not primarily associated with juvenile growth phases or tree age in general, but may also be associated with temporal disturbances of $\delta^2\text{H}_{\text{sw}}$ among the four tree sampling sites. A plausible mechanism would be a changing relationship between $\delta^2\text{H}_{\text{precip}}$ and $\delta^2\text{H}_{\text{sw}}$ over time in the nearby tree environment, such as changing soil and hydrological properties (leading to varying source water accumulation). A better understanding of such occasional temporal trend deviations in $\delta^2\text{H}_{\text{LM}}$ may improve sampling strategies. Trees with potential temporal disturbances in the $\delta^2\text{H}_{\text{sw}}-\delta^2\text{H}_{\text{LM}}$ relationship may justifiably be excluded when producing a mean $\delta^2\text{H}_{\text{LM}}$ chronology subsequently leading to an improved overall coherency. Nonetheless, the $\delta^2\text{H}_{\text{LM}}$ values of the nine tree-ring series generally show strong coherency and no major influence related to tree age. Therefore, we developed a chronology (without conducting any detrending or correction method) for the common period 1916–2015 by calculating for each of the nine tree-ring series the annual $\delta^2\text{H}_{\text{LM}}$ deviation to the mean of the 1961–1990 period. Subsequently, by integrating all nine $\delta^2\text{H}_{\text{LM}}$ series, a mean chronology was calculated with 95% confidence intervals to account for the internal variability (Fig. 5).

4.3. Relationship between $\delta^2\text{H}_{\text{LM}}$ chronology and local $\delta^2\text{H}_{\text{precip}}$ and climate

For the 1971–2008 period, correlations between the $\delta^2\text{H}_{\text{LM}}$ chronology and $\delta^2\text{H}_{\text{precip}}$ signatures are insignificant when using single months except for June ($r = 0.43$, $p < 0.01$; Fig. 6a). Correlations partly increase in magnitude when using averaged $\delta^2\text{H}_{\text{precip}}$ values of

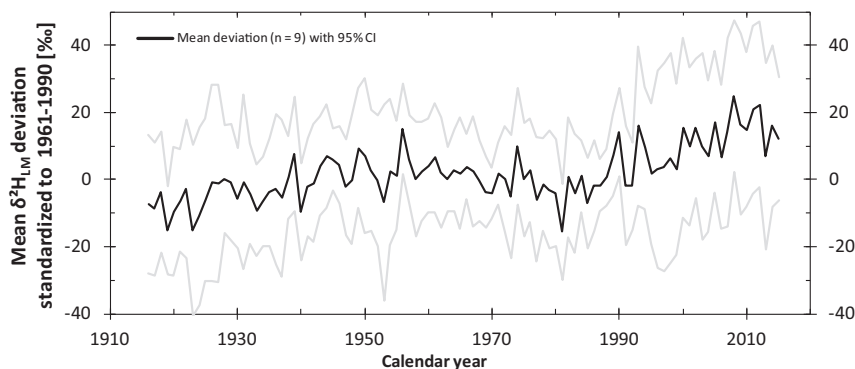


Fig. 5. δ^2H_{LM} chronology for the 1916–2015 common period. Chronology reflects the arithmetic mean of the annual δ^2H_{LM} deviations with respect to the 1961–1990 period of the nine individual tree-ring series and is shown with 95% confidence intervals (grey lines).

the previous fall, previous winter, spring and summer ($r = 0.40, 0.42, 0.53, \text{ and } 0.45$, respectively; $p < 0.01$). Highest r values are, however, found when using annual integrals, such as January until December with $r = 0.66$ ($p < 0.001$) or previous September to current August with $r = 0.73$ ($p < 0.001$; Fig. 6a and Supplemental Fig. S3). The observed pattern of the estimated correlation coefficients (r values increase when extending the temporal integral of δ^2H_{precip} values) clearly indicates that tree's source water rather reflects an accumulation of multiple months to seasons and agrees with earlier findings (Allen et al., 2019; Ehleringer and Dawson, 1992; Feng and Epstein, 1995; Tang et al., 2000). Recent investigations supported this particularly for *F. sylvatica* because they primarily use water from deeper soil layers (40 to 50 cm; Goldsmith et al., 2019) with δ^2H values less prone to changes induced by single precipitation events. Furthermore, tree-ring growth of *F. sylvatica* typically starts in April and ceases in August (Čufar et al., 2008; Michelot et al., 2012) or September (Kraus et al., 2016). Precipitation falling after the latest late wood formation may therefore

only contribute to the tree source water of the following year. Hence, the δ^2H_{LM} chronology not only correlates best with the 'shifted' annual values (previous September to current August), but this time period is also supported by considerations in source water accumulation and tree-ring growth. Conclusively, the δ^2H_{LM} chronology is considered to reflect primarily mean annual δ^2H_{precip} values (previous September to current August) for the 1971–2008 period of data overlap. For the remaining years of the full 1916–2015 period, care has to be taken when the relative contribution of seasonal precipitation to the annual amount changes. In that case, δ^2H_{LM} would reflect a more seasonally pronounced δ^2H_{precip} signature. However, even though this induces some noise into the δ^2H_{precip} - δ^2H_{LM} relationship, we consider this influence as negligible for Hohenpeißenberg since neither annual nor seasonal precipitation amount changed significantly over 1916–2015 (cf. Section 2).

When comparing the δ^2H_{LM} chronology with temperature data of the nearby DWD station (covering the full period of 1916–2015), highly

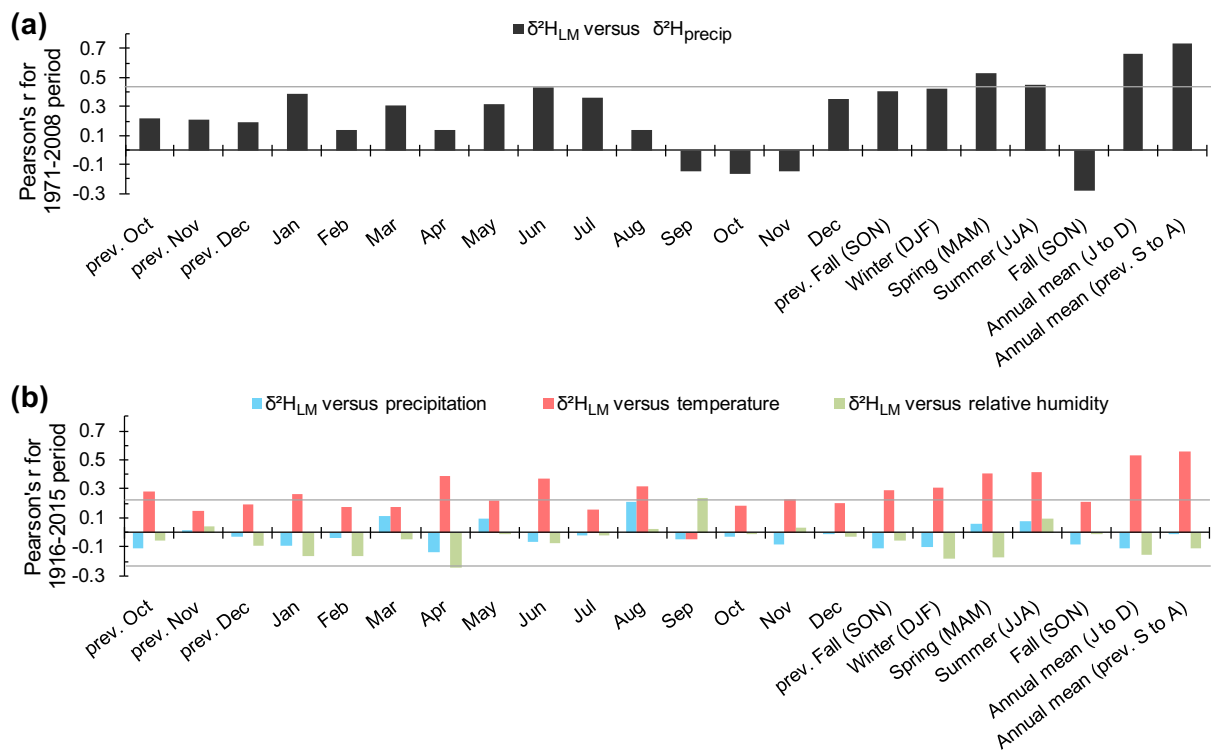


Fig. 6. Pearson's correlations (r) between annually resolved mean δ^2H_{LM} chronology (cf. Fig. 5) and δ^2H_{precip} from 1971 to 2008 ($n = 36$) (a) as well as with temperature, precipitation and relative humidity from 1916 to 2015 ($n = 100$) (b) for Hohenpeißenberg (Germany). Grey horizontal lines mark significance level of 99.9%.

significant correlations ($p < 0.01$) are found for numerous months (previous October, January, April, June, August) with r values ranging from 0.26 to 0.39 and for all seasons except for fall of the current year with r values ranging from 0.29 to 0.41 (Fig. 6b). Similar as observed for $\delta^2\text{H}_{\text{precip}}$, the highest correlation coefficient can, however, be noted for the ‘shifted’ annually averaged temperature (year defined from previous September to August) with $r = 0.56$ ($p < 0.001$). Precipitation amount as well as relative humidity show weak correlations with the $\delta^2\text{H}_{\text{LM}}$ chronology (Fig. 6b) and are mostly insignificant.

4.4. Relationship between the $\delta^2\text{H}_{\text{LM}}$ chronology and large-scale climate and the NAO

Besides changes in local climate, $\delta^2\text{H}_{\text{precip}}$ at the site of precipitation is controlled by a number of large-scale and remote hydro-climatic influences. This includes changing meteorological conditions in the moisture source area, meridional atmospheric transport and particularly a modified water volume loss, but also potential mixing with different air masses (Araguás-Araguás et al., 2000; Dansgaard, 1964; Rozanski et al., 1993). Stable water isotopes are therefore increasingly considered to indicate large-scale atmospheric phenomena rather than variations in local or regional climate state (Bowen et al., 2019) including atmospheric circulation modes such as the NAO index (Baldini et al., 2008; Deininger et al., 2016; Field, 2010).

As the $\delta^2\text{H}_{\text{LM}}$ chronology reflects best annually averaged $\delta^2\text{H}_{\text{precip}}$ values (previous-year September to current-year August), spatial correlations have been accordingly estimated between the Hohenpeißenberg $\delta^2\text{H}_{\text{LM}}$ chronology and mean annual surface temperatures (previous-year September to current-year August). The results show significance across Western Europe (r ranging from 0.2 to > 0.6 with $p < 0.1$; Fig. 7a). Highest correlations (with $r > 0.6$) are found for both land (northern Mediterranean) and numerous sea areas (western Mediterranean Sea, northwest North Sea, Gulf of Biscaya, parts of the eastern North Atlantic and the Arctic Sea). This shows that the $\delta^2\text{H}_{\text{LM}}$ chronology exhibits higher correlations with temperature anomalies of multiple remote areas than with local temperature anomalies at Hohenpeißenberg (Fig. 6b). A similar evaluation of temperature influences on the temporal variability of stable water isotopes was done by Field (2010) using data of 23 central European GNIP stations. Therein, spatial correlations between temperature and stable water isotopes showed a similar multi-centered structure with areas of highest correlations west of the used GNIP stations. Correlations between the $\delta^2\text{H}_{\text{LM}}$ chronology and the NAO index are insignificant regardless of the used monthly or averaged winter NAO index (Fig. 7b). Based on the found temporal integral of accumulated soil water at Hohenpeißenberg (previous September to current August; Fig. 6a), the lacking influence of the NAO on the $\delta^2\text{H}_{\text{LM}}$ chronology may not surprise. Correlations between the NAO and stable water isotopes have mainly been reported during winter (Baldini et al., 2008; Field, 2010) including also the Hohenpeißenberg study site (Deininger et al., 2016). Overall, the $\delta^2\text{H}_{\text{LM}}$ chronology reflects climatic imprints commonly observed for central European stable water isotopes. Moreover, a lacking sensitivity for the NAO is further evidence that $\delta^2\text{H}_{\text{LM}}$ values record primarily an annual integration of $\delta^2\text{H}_{\text{precip}}$ values.

The main moisture source of precipitation of the northern Alpine foothills (including the Hohenpeißenberg study site) has been determined by Lagrangian moisture source diagnostics for the time period 1995–2002 (Sodemann and Zubler, 2010). This study concludes that the majority of annual northern Alpine precipitation originates from multiple sources including the eastern North Atlantic (~29%), continental Europe (~21%), the Western Mediterranean Sea (~16%), the North and Baltic Sea (~13%) and the Arctic and Nordic Seas (~5%). Consequently, even though our $\delta^2\text{H}_{\text{LM}}$ chronology shows highly significant correlations with large-scale and remote annual temperature changes, the involved stable water isotope mechanisms on Hohenpeißenberg $\delta^2\text{H}_{\text{precip}}$ values are more complex considering the

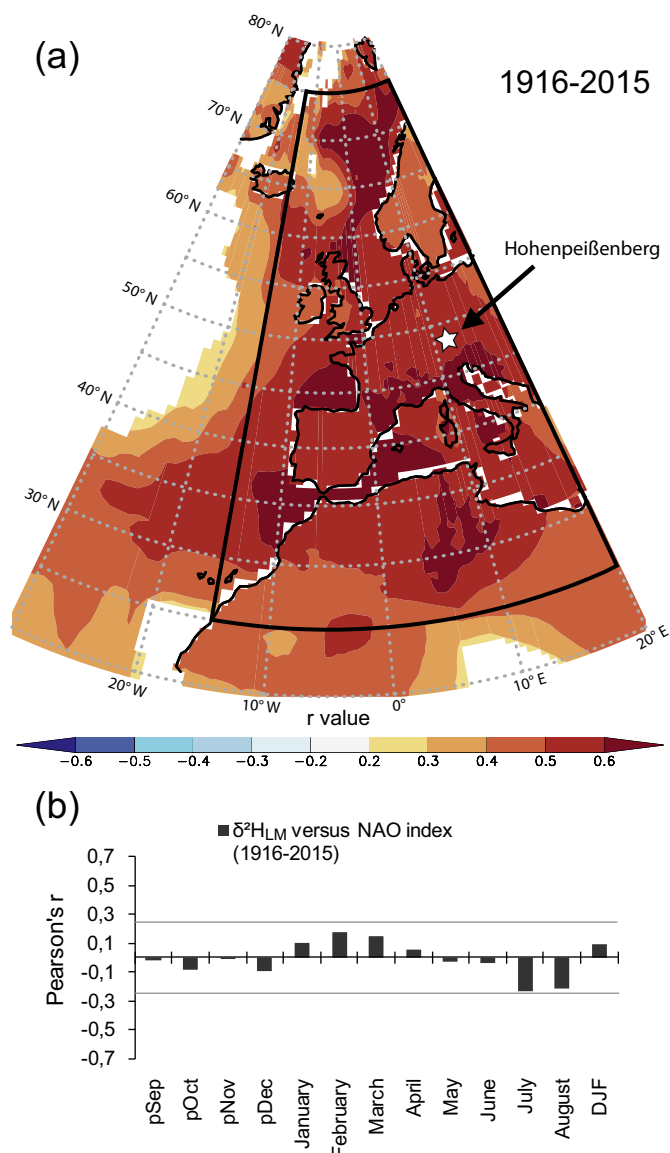


Fig. 7. (a) Spatial correlations between inter-annually resolved land and sea surface temperature changes (previous September to current August; CRUT4.01 and HadSST1) and mean $\delta^2\text{H}_{\text{LM}}$ chronology from Hohenpeißenberg (Germany) for the time period 1916–2015. Only correlations with significance $p < 0.05$ are shown. Black box covers areas of highest correlations ($r > 0.6$). White star marks the Hohenpeißenberg study site in Germany. (b) Pearson's r between the $\delta^2\text{H}_{\text{LM}}$ chronology and the NAO index (Jones et al., 1997). DJF marks the correlation with the averaged winter NAO index commonly observed to influence winter stable water isotope variability in Europe (Baldini et al., 2008; Deininger et al., 2016; Field, 2010). Grey horizontal lines mark significance level of 99.9%.

multiple moisture source areas of northern Alpine precipitation and the associated numerous hydro-climatic influences therein. A dominant control on inter-annual variability of stable water isotopes comes from variations in the Rayleigh distillation (Gat, 1996). This process describes the progressive ^2H depletion of the remaining atmospheric vapor as a result of consecutive rainouts along the air mass trajectory. Consequently, the Rayleigh distillation alters primarily as a function of the temperature gradient between the moisture source areas and the site of precipitation. Interestingly, northern Alpine moisture source areas (Sodemann and Zubler, 2010) overlap broadly with areas where temperature changes show the highest correlations with the Hohenpeißenberg $\delta^2\text{H}_{\text{LM}}$ chronology ($r > 0.6$; Fig. 7a). Therefore, the

positive correlation areas (Fig. 7a) may point to a potential linkage between rising temperatures in the moisture source areas and a less intense Rayleigh distillation leading to higher $\delta^2\text{H}_{\text{precip}}$ values at Hohenpeißenberg.

4.5. Western European surface temperature changes as main control for the $\delta^2\text{H}_{\text{LM}}$ chronology?

To assess the temporal stability of the found large-scale temperature influence on central European stable isotopes, we attempt to reconstruct averaged surface temperatures changes of the area enclosing the highest spatial correlations ($r > 0.6$; $15^\circ\text{W} - 20^\circ\text{E}$; $25-75^\circ\text{N}$; black box in Fig. 7a). We developed a linear regression model between the annually averaged (previous September to August) Western European surface temperature (WEST) anomaly and the $\delta^2\text{H}_{\text{LM}}$ chronology. The model reveals a significant correlation ($r = 0.72$; $p < 0.001$, $DW = 1.4$) with an elevated r value when compared to any of the observed correlations shown in Fig. 7. When expressing the linear regression model, the following equation is obtained:

$$\Delta\text{Temperature}_{\text{WEST}} [^\circ\text{C}] \approx (\Delta\delta^2\text{H}_{\text{LM}} [\text{‰}] + 0.75)/13.66 [^\circ\text{C}/\text{‰}] \quad (1)$$

We subsequently compared the reconstructed and instrumental WEST anomalies at annual resolution (Fig. 8). To account for errors induced by the internal $\delta^2\text{H}_{\text{LM}}$ variability of the nine tree-ring series, we converted the annually estimated 95% confidence interval (error bars in Fig. 5) into temperature using Eq. (1). As an additional error assessment, we calculated the differences of the reconstructed and instrumental WEST anomalies that result at annual resolution (Fig. 8b). Differences between annually reconstructed and instrumental WEST anomalies differ in the range of -0.9 to $+1.3$ $^\circ\text{C}$ with an average

absolute deviation of 0.3 $^\circ\text{C}$ ($n = 100$) (Fig. 8b). Hence, for the broad majority of annual reconstructions ($n = 84$), absolute deviations are < 0.5 $^\circ\text{C}$, whereby the remaining absolute deviations in annual reconstructions are either between 0.5 and 1.0 ($n = 14$) and highest in 1956 and 1993.

When conducting a split calibration/verification on the linear model (Eq. (1)), a rather weak temporal robustness is indicated (1916–1965: $CE = -1.52$, $RE = -0.73$; 1966–2015: $CE = 0.12$, $RE = -0.79$). To explore this issue in more detail, we calculated a moving correlation for 31-year segments (blue line in Fig. 8c). The beginning of the chronology shows r values ranging between 0.4 and 0.6 until the segment centered at 1940. After that, r values decrease and remain distinctively lower (ranging between 0.2 and 0.4) until the segment centered at 1972. In the following, r values increase again to values ranging between 0.5 and 0.8 until the end of the chronology. The phase of low moving correlations begins and ends rather abruptly also centering around 1956. This year, showing the highest deviation between reconstructed and instrumental WEST anomalies ($\Delta + 1.3$ $^\circ\text{C}$; Fig. 8b), substantially lowers the overall performance of our linear model. Interestingly, during February 1956, central and western European weather was affected by an extreme abnormality in hemispheric circulation patterns (Andrews, 1956; Dizerens et al., 2017). Due to a long-lasting blocking of the westerlies, cold polar air continuously advected into Western and Central Europe resulting, for instance, in the coldest month ever recorded (-12 $^\circ\text{C}$) at Hohenpeißenberg. Besides this severe temperature drop, such a reverse atmospheric circulation undoubtedly shifts moisture source areas and associated air mass trajectories of central European precipitation. As a result, $\delta^2\text{H}_{\text{precip}}$ values of 1956 may have been extraordinary causing a strong deviation from the commonly found association with WEST anomalies.

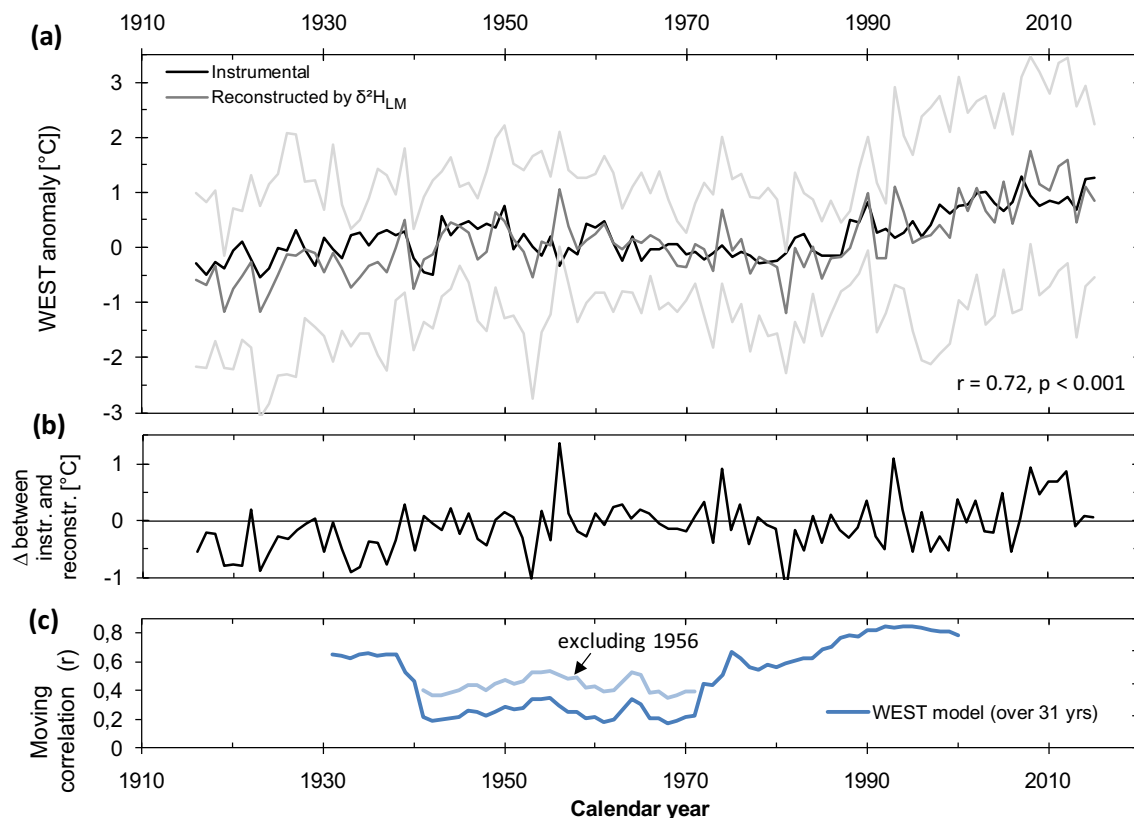


Fig. 8. a) Instrumental and reconstructed WEST anomaly (using Eq. (1)) for the time period 1916–2015 at annual resolution. Eq. (1) was also used to convert the annually estimated 95% confidence interval into temperature (grey lines) to account for errors induced by the internal $\delta^2\text{H}_{\text{LM}}$ variability of the nine tree-ring series b) Difference between reconstructed and instrumental WEST anomaly at annual resolution. c) Moving correlation between WEST anomalies and the $\delta^2\text{H}_{\text{LM}}$ chronology (using 31-year segments; blue line) along with the equivalent moving correlations when excluding the year 1956 (pale blue line). (For interpretation of the references to color in this figure legend, the reader is referred to the web version of this article.)

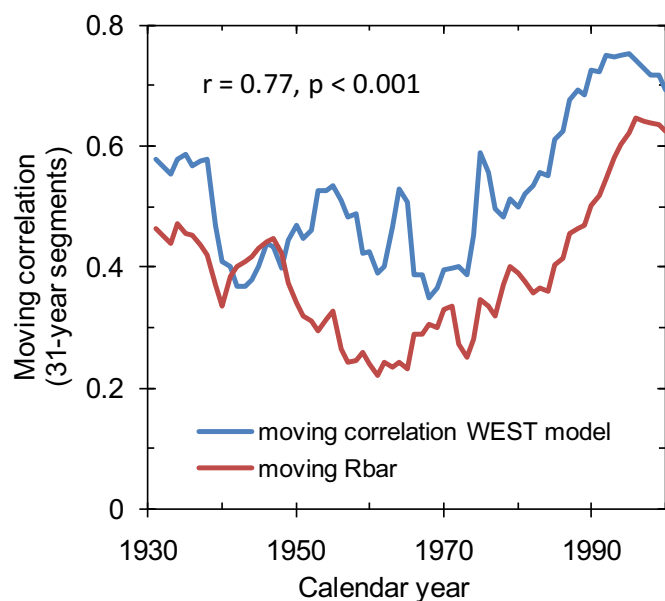


Fig. 9. Moving correlation between WEST anomalies and the $\delta^2\text{H}_{\text{LM}}$ chronology (blue line) along with the moving Rbar value (red line). Both moving metrics use 31-year segments and correlate with $r = 0.77$. (For interpretation of the references to color in this figure legend, the reader is referred to the web version of this article.)

Calculating moving correlations between WEST anomalies and the $\delta^2\text{H}_{\text{LM}}$ chronology without the year 1956 notably improves the temporal robustness of the linear model (pale blue line in Fig. 8c). Nonetheless, moving correlations remain systematically lower during the central part of our chronology. Besides extreme atmospheric events modifying the relationship between temperature and stable water isotopes, the reconstruction skill may additionally be influenced by inconsistencies between $\delta^2\text{H}_{\text{precip}}$ and $\delta^2\text{H}_{\text{LM}}$ values. Support for this is

given as the period of low moving correlation broadly resembles the one observed for the moving Rbar value indicating a decrease in coherency among the nine $\delta^2\text{H}_{\text{LM}}$ tree-ring series (both moving correlations are shown in Fig. 9). In fact, both parameters correlate significantly ($r = 0.77$, $p < 0.001$) suggesting that changes in the moving correlation are mainly controlled by the internal coherency (Rbar). We again created spatial correlations between large-scale temperature changes and the $\delta^2\text{H}_{\text{LM}}$ chronology for three separate periods (Fig. 10). To assure comparability, we chose three equal periods (1916–1948, 1949–1982 and 1983–2015), whereby the second period also broadly isolates the observed period of the lowest moving correlations (Fig. 8c). Whereas the beginning and the end of our chronology (1916–1948 and 1983–2015, respectively) show significant correlations for large areas across Europe (Fig. 10a, c), the central part (1949–1982) appears almost insensitive to European temperature changes. At the same time, reversed relationships become apparent in northern Africa (Fig. 10b). Estimating Rbar values for each of these periods, indicates the lowest value for the central third (0.29) revealing a similar pattern as observed for the moving Rbar values. Thus, during the 1949–1982 period, the internal coherency of the $\delta^2\text{H}_{\text{LM}}$ chronology seems insufficient to accurately record local $\delta^2\text{H}_{\text{precip}}$ changes and is consequently unable to record the climatic imprint therein.

Comparing the climate-sensitive periods 1916–1948 and 1983–2015 in detail (cf. Fig. 10b and c) shows further that areas of highest correlations move partly eastwards with time leading to an enlarged coverage of European land masses and, consequently, indicates that local Hohenpeißenberg temperatures are only significant for the most recent 1983–2015 period. As $\delta^2\text{H}_{\text{precip}}$ changes also integrate alterations in large-scale atmospheric circulation patterns, the eastward movement of areas of highest correlation may indicate an equivalent movement of moisture source areas and the associated air mass trajectories of northern Alpine precipitation during the 20th century (moving from the European shelf to Western and Central Europe). However, contrary to the year 1956, the indicated modification in atmospheric circulation patterns between these two periods seems to have no major impact on the linear model as indicated by the

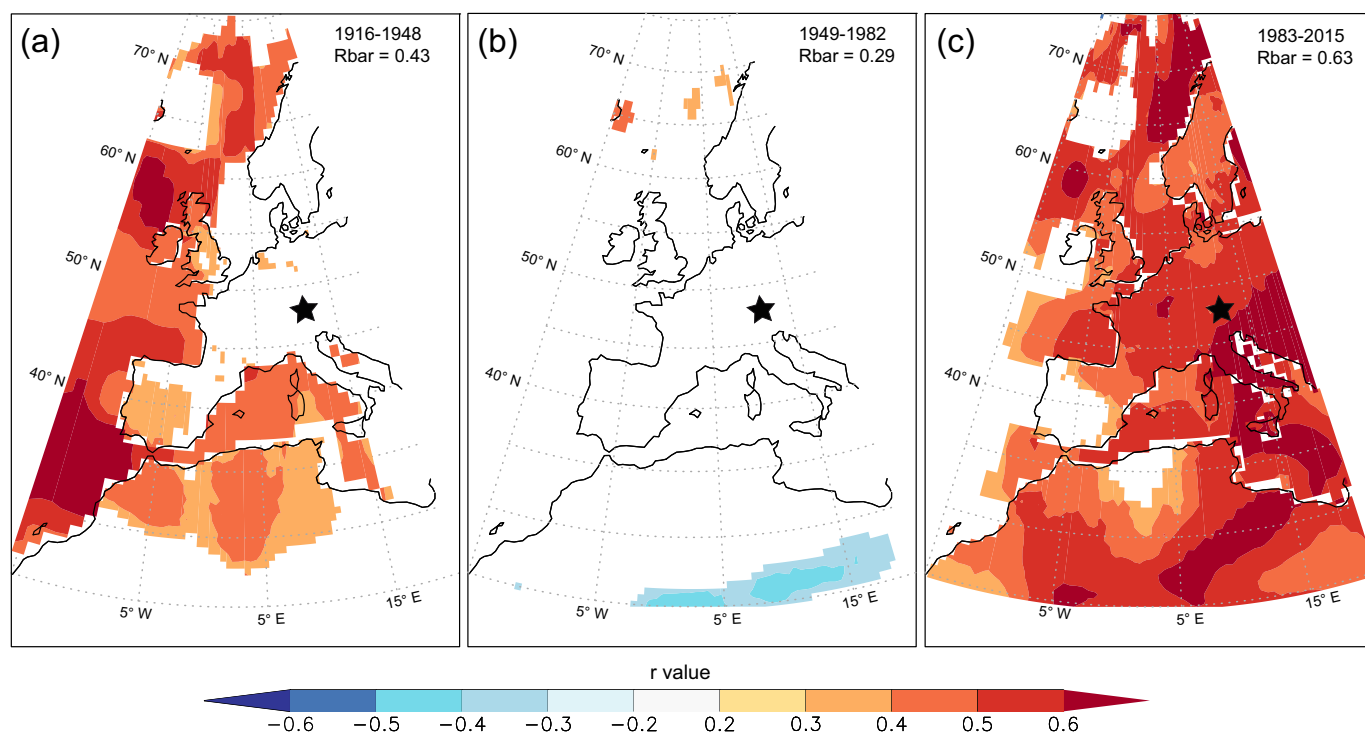


Fig. 10. Spatial correlations between surface temperature changes and the $\delta^2\text{H}_{\text{LM}}$ chronology for three time periods (a) 1916–1948, (b) 1949–1982 and (c) 1983–2015. Same data used as in Fig. 7a. Hohenpeißenberg study site is marked by black star.

elevated moving correlations for both these periods (Fig. 8c).

Conclusively, the $\delta^2\text{H}_{\text{LM}}$ chronology reflects primarily annually $\delta^2\text{H}_{\text{precip}}$ values and, consequently, shows commonly observed climatic imprints for central European stable water isotopes (particularly large-scale and remote temperature changes; Field, 2010). Despite the complex evolution of northern Alpine $\delta^2\text{H}_{\text{precip}}$ changes, the $\delta^2\text{H}_{\text{LM}}$ chronology and the produced simple linear regression model suggest that the variance can mainly be explained by WEST anomalies ($r^2 = 0.52$). Nonetheless, even though this model demonstrates potential of applying tree-ring $\delta^2\text{H}_{\text{LM}}$ values for reconstructing large-scale temperature changes, it also reveals its current constraints. The temporal robustness of the found temperature influence seems sensitive to low Rbar values but also to changing atmospheric circulation patterns occurring on short and long-term scales. Thus, besides an improved understanding of occasional temporal inconsistencies among tree-ring $\delta^2\text{H}_{\text{LM}}$ values, future studies may also involve a critical assessment of the influence of changing atmospheric circulation patterns on the relationship between large-scale temperatures and $\delta^2\text{H}_{\text{precip}}$ values. Alternatively, when combined with other temperature reconstructions, tree-ring $\delta^2\text{H}_{\text{LM}}$ values may also serve as proxy for synoptic climate changes such as reversed atmospheric circulations patterns and/or shifts in moisture source areas.

5. Conclusions

This study provides the first comprehensive investigation of the relationship between inter-annually resolved $\delta^2\text{H}_{\text{LM}}$ values, instrumental $\delta^2\text{H}_{\text{precip}}$ as well as local and large-scale climate data by using nine annually resolved *F. sylvatica* tree-ring series collected at Hohenpeißenberg (Germany). Tree-ring $\delta^2\text{H}_{\text{LM}}$ series reveal valuable features when applied as a paleoclimate proxy. This includes a strong overall internal coherency and no indication of non-climatic (age related) trends affecting the $\delta^2\text{H}_{\text{LM}}$ variability. A subsequently produced averaged $\delta^2\text{H}_{\text{LM}}$ chronology (integrating the nine tree-ring series covering the 1916–2015 period) was found to reflect primarily annual $\delta^2\text{H}_{\text{precip}}$ values averaged over the period previous-year September to current-year August. This finding agrees with considerations in local source water accumulation and seasonal tree-ring growth of *F. sylvatica*.

In line with the found association with $\delta^2\text{H}_{\text{precip}}$ values, the $\delta^2\text{H}_{\text{LM}}$ chronology shows similar climatic imprints as commonly observed for central European stable water isotopes values including a dominant influence of large-scale and remote temperature changes. In an attempt to reconstruct annual temperature anomalies averaged over Western Europe using the $\delta^2\text{H}_{\text{LM}}$ chronology, a linear model showed a significant relationship ($r = 0.72$, $p < 0.001$, $n = 100$). The temporal robustness of this linear relationship revealed, however, important insights when applying tree-ring $\delta^2\text{H}_{\text{LM}}$ values for climate reconstructions. The internal coherency among the tree-ring proxy data can vary over time and potentially prevents an accurate recording of the climate-sensitive $\delta^2\text{H}_{\text{precip}}$ values. Here, indication was found that persistently low moving Rbar values (using 31-years period) of lower than 0.4 obliterate the commonly observed relationship between Western European temperature changes and the $\delta^2\text{H}_{\text{LM}}$ chronology. Reconstruction models may therefore benefit from an improved understanding of the internal mechanisms controlling stable hydrogen isotope fractionation during lignin methoxyl biosynthesis. Future studies may also evaluate sub-annual variability of $\delta^2\text{H}_{\text{LM}}$ values. Such differences would induce noise in the $\delta^2\text{H}_{\text{precip}}$ - $\delta^2\text{H}_{\text{LM}}$ relationship particularly when ratios between early- and latewood width differ over time.

Besides temporal inconsistencies in the $\delta^2\text{H}_{\text{precip}}$ - $\delta^2\text{H}_{\text{LM}}$ relationship, our model also suggests that the large-scale temperature influence on $\delta^2\text{H}_{\text{precip}}$ requires a somewhat uniform mode of atmospheric circulation. Hence, tree-ring $\delta^2\text{H}_{\text{LM}}$ values may particularly powerful in combination with other temperature proxies such as TRW and MXD to differentiate between temperature and meteorological controls.

Moreover, instrumental stable water isotope data usually covers only a few decades and are very sparse prior the 1960's (IAEA/WMO, 2020). Thus, besides a direct application for paleoclimate and -hydrology reconstructions, tree-ring $\delta^2\text{H}_{\text{LM}}$ values may also be a valuable tool to decipher climatic controls on the inter-annual variability of $\delta^2\text{H}_{\text{precip}}$ values.

Data availability

$\delta^2\text{H}_{\text{LM}}$ measurements of the nine tree-ring core are available in the Supplemental Table S1. Other data used in this publication are available to the community and can be accessed by request to the corresponding author.

Declaration of competing interest

The authors declare no competing financial interests.

Acknowledgments

This study was supported by the German Research Foundation (DFG: AN1191/3-1, KE884/6-2, KE884/6-3, KE884/8-1 and KE884/8-2, SCHO 1274/13-1). We gratefully thank Moritz Schroll and Hendric Glatting for supporting field campaigns.

Appendix A. Supplementary data

Supplementary data to this article can be found online at <https://doi.org/10.1016/j.palaeo.2020.109665>.

References

- Allen, S.T., Kirchner, J.W., Braun, S., Siegwolf, R.T.W., Goldsmith, G.R., 2019. Seasonal origins of soil water used by trees. *Hydrol. Earth Syst. Sci.* 23, 1199–1210. <https://doi.org/10.5194/hess-23-1199-2019>.
- Allison, G.B., 1982. The relationship between 18O and deuterium in water in sand columns undergoing evaporation. *J. Hydrol.* 55, 163–169. [https://doi.org/10.1016/0022-1694\(82\)90127-5](https://doi.org/10.1016/0022-1694(82)90127-5).
- Anderson, W.T., Bernasconi, S.M., McKenzie, J.A., Saurer, M., 2002. Anderson et al, 2002 - Model evaluation for reconstructing the oxygen isotopic composition in precipitation from tree ring cellulose over the last century – *Chem. Geol.* pdf 121–137.
- Andrews, J.F., 1956. The Weather and circulation of February 1956. *Mon. Weather Rev.* 84, 66–74. [https://doi.org/10.1175/1520-0493\(1956\)084<0066:TWACOF>2.0.CO;2](https://doi.org/10.1175/1520-0493(1956)084<0066:TWACOF>2.0.CO;2).
- Anhäuser, T., Greule, M., Keppler, F., 2017a. Stable hydrogen isotope values of lignin methoxyl groups of four tree species across Germany and their implication for temperature reconstruction. *Sci. Total Environ.* 579, 263–271. <https://doi.org/10.1016/j.scitotenv.2016.11.109>.
- Anhäuser, T., Greule, M., Polag, D., Bowen, G.J., Keppler, F., 2017b. Mean annual temperatures of mid-latitude regions derived from $\delta^2\text{H}$ values of wood lignin methoxyl groups and its implications for paleoclimate studies. *Sci. Total Environ.* 574, 1276–1282. <https://doi.org/10.1016/j.scitotenv.2016.07.189>.
- Anhäuser, T., Hook, B.A., Halfar, J., Greule, M., Keppler, F., 2018. Earliest Eocene cold period and polar amplification - Insights from $\delta^2\text{H}$ values of lignin methoxyl groups of mummified wood. *Palaeogeogr. Palaeoclimatol. Palaeoecol.* 505, 326–336. <https://doi.org/10.1016/j.palaeo.2018.05.049>.
- Araguas-Araguas, L., Froehlich, K., Rozanski, K., 2000. Deuterium and oxygen-18 isotope composition of precipitation and atmospheric moisture. *Hydrol. Process.* 14, 1341–1355. [https://doi.org/10.1002/1099-1085\(20000615\)14:8<1341::aid-hyp983>3.0.co;2-z](https://doi.org/10.1002/1099-1085(20000615)14:8<1341::aid-hyp983>3.0.co;2-z).
- Araguas-Araguas, L., Froehlich, K., Rozanski, K., 2000. Deuterium and oxygen-18 isotope composition of precipitation and atmospheric moisture. *Hydrological Processes* 1341–1355. [https://doi.org/10.1002/1099-1085\(20000615\)14:8<1341::AID-HYP983>3.3.CO;2-Q](https://doi.org/10.1002/1099-1085(20000615)14:8<1341::AID-HYP983>3.3.CO;2-Q).
- Augusti, A., Betson, T.R., Schleucher, J., 2006. Hydrogen exchange during cellulose synthesis distinguishes climatic and biochemical isotope fractionations in tree rings. *New Phytol.* 172, 490–499. <https://doi.org/10.1111/j.1469-8137.2006.01843.x>.
- Augusti, A., Betson, T.R., Schleucher, J., 2008. Deriving correlated climate and physiological signals from deuterium isotopomers in tree rings. *Chem. Geol.* 252, 1–8. <https://doi.org/10.1016/j.chemgeo.2008.01.011>.
- Baldini, L.M., McDermott, F., Foley, A.M., Baldani, J.U.L., 2008. Spatial variability in the European winter precipitation δ 18O-NAO relationship: Implications for reconstructing NAO-mode climate variability in the Holocene. *Geophys. Res. Lett.* 35. <https://doi.org/10.1029/2007GL032027>.
- Boerjan, W., Ralph, J., Baucher, M., 2003. Lignin biosynthesis. *Annu. Rev. Plant Biol.* 54, 519–546. <https://doi.org/10.1146/annurev.arplant.54.031902.134938>.

- Bowen, G.J., Cai, Z., Fiorella, R.P., Putman, A.L., 2019. Isotopes in the water cycle: regional- to global-scale patterns and applications. *Annu. Rev. Earth Planet. Sci.* 47, 453–479. <https://doi.org/10.1146/annurev-earth-053018-060220>.
- Briffa, K.R., Jones, P.D., Pilcher, J.R., Hughes, M.K., 1988. Reconstructing summer temperatures in Northern Fennoscandia back to A.D. 1700 using tree-ring data from Scots pine. *Arct. Alp. Res.* 20, 385–394.
- Bunn, A.G., 2008. A dendrochronology program library in R (dplR). *Dendrochronologia* 26, 115–124. <https://doi.org/10.1016/j.dendro.2008.01.002>.
- Büntgen, U., Tegel, W., Nicolussi, K., McCormick, M., Frank, D., Trouet, V., Kaplan, J.O., Herzog, F., Heussner, K.-U., Wanner, H., Luterbacher, J., Esper, J., 2011. 2500 years of European climate variability and human susceptibility. *Science* 331, 578–582. <https://doi.org/10.1126/science.1197175>.
- Cook, E.R., 1994. Spatial regression methods in dendroclimatology: a review and comparison of two techniques. *Int. J. Climatol.* 14, 379–402.
- Čufar, K., Prislan, P., De Luis, M., Gričar, J., 2008. Tree-ring variation, wood formation and phenology of beech (*Fagus sylvatica*) from a representative site in Slovenia, SE Central Europe. *Trees - Struct. Funct.* 22, 749–758. doi:<https://doi.org/10.1007/s00468-008-0235-6>.
- Cullen, L.E., Grierson, P.F., 2006. Is cellulose extraction necessary for developing stable carbon and oxygen isotopes chronologies from *Callitris glaucophylla*? *Palaeogeogr. Palaeoclimatol. Palaeoecol.* 236, 206–216. <https://doi.org/10.1016/j.palaeo.2005.11.003>.
- Dansgaard, W., 1964. Stable isotopes in precipitation. *Tellus* 16, 436–468. <https://doi.org/10.3402/tellusa.v16i4.8993>.
- Deininger, M., Werner, M., McDermott, F., 2016. North Atlantic Oscillation controls on oxygen and hydrogen isotope gradients in winter precipitation across Europe; Implications for palaeoclimate studies. *Clim. Past* 12, 2127–2143. <https://doi.org/10.5194/cp-12-2127-2016>.
- DeNiro, M.J., 1981. The effects of different methods of preparing cellulose nitrate on the determination of the D/H ratios of non-exchangeable hydrogen of cellulose. *Earth Planet. Sci. Lett.* 54, 177–185. [https://doi.org/10.1016/0012-821X\(81\)90001-7](https://doi.org/10.1016/0012-821X(81)90001-7).
- Dizerens, C., Lenggenhager, S., Schwander, M., Buck, A., Foffa, S., 2017. The 1956 Cold Wave in Western Europe. *Geogr. Bernensia* G92, 101–111. <https://doi.org/10.4480/GB2017.G92.09>.
- Ehleringer, J.R., Dawson, T.E., 1992. Water uptake by plants: perspectives from stable isotope composition. *Plant Cell Environ.* 15, 1073–1082. <https://doi.org/10.1111/j.1365-3040.1992.tb01657.x>.
- Eliáš, P., Kratochvílová, I., Janouš, D., Marek, M., Masarovičová, E., 1989. Stand microclimate and physiological activity of tree leaves in an oak-hornbeam forest. *Trees* 3, 227–233. <https://doi.org/10.1007/BF00225356>.
- Epstein, S., Yapp, C.J., Hall, J.H., 1976. The determination of the D/H ratio of non-exchangeable hydrogen in cellulose extracted from aquatic and land plants. *Earth Planet. Sci. Lett.* 30, 241–251. [https://doi.org/10.1016/0012-821X\(76\)90251-X](https://doi.org/10.1016/0012-821X(76)90251-X).
- Esper, J., Cook, E.R., Schweingruber, F.H., 2002. Low-frequency signals in long tree-ring chronologies for reconstructing past temperature variability. *Science* 295, 2250–2253. <https://doi.org/10.1126/science.1066208>.
- Esper, J., Frank, D.C., Battipaglia, G., Büntgen, U., Holert, C., Treydte, K., Siegwolf, R., Saurer, M., 2010. Low-frequency noise in $\delta^{13}C$ and $\delta^{18}O$ tree ring data: a case study of *Pinus uncinata* in the Spanish Pyrenees. *Glob. Biogeochem. Cycles* 24, 1–11. <https://doi.org/10.1029/2010GB003772>.
- Esper, J., Krusic, P.J., Ljungqvist, F.C., Luterbacher, J., Carrer, M., Cook, E., Davi, N.K., Hartl-Meier, C., Kiryanov, A., Konter, O., Myglan, V., Timonen, M., Treydte, K., Trouet, V., Villalba, R., Yang, B., Büntgen, U., 2016. Ranking of tree-ring based temperature reconstructions of the past millennium. *Quat. Sci. Rev.* 145, 134–151. <https://doi.org/10.1016/j.quascirev.2016.05.009>.
- Esper, J., Klippel, L., Krusic, P.J., Konter, O., Raible, C.C., Xoplaki, E., Luterbacher, J., Büntgen, U., 2019. Eastern Mediterranean summer temperatures since 730 CE from Mt. Smolikas tree-ring densities. *Clim. Dyn.* <https://doi.org/10.1007/s00382-019-05063-x>.
- Feakins, S.J., Ellsworth, P.V., Sternberg, L. da S.L., 2013. Lignin methoxyl hydrogen isotope ratios in a coastal ecosystem. *Geochim. Cosmochim. Acta* 121, 54–66. <https://doi.org/10.1016/j.gca.2013.07.012>.
- Feng, X., Epstein, S., 1995. Climatic temperature records in δD data from tree rings. *Geochim. Cosmochim. Acta* 59, 3029–3037. [https://doi.org/10.1016/0016-7037\(95\)00192-1](https://doi.org/10.1016/0016-7037(95)00192-1).
- Feng, X., Krishnamurthy, R.V., Epstein, S., 1993. Determination of D/H ratios of non-exchangeable hydrogen in cellulose: a method based on the cellulose-water exchange reaction. *Geochim. Cosmochim. Acta* 57, 4249–4256. [https://doi.org/10.1016/0016-7037\(93\)90320-V](https://doi.org/10.1016/0016-7037(93)90320-V).
- Field, R.D., 2010. Observed and modeled controls on precipitation $\delta^{18}O$ over Europe: from local temperature to the Northern Annular Mode. *J. Geophys. Res. Atmos.* 115, 1–14. <https://doi.org/10.1029/2009JD013370>.
- Gärtner, H., Nievergelt, D., 2010. The core-microtome: a new tool for surface preparation on cores and time series analysis of varying cell parameters. *Dendrochronologia* 28, 85–92. <https://doi.org/10.1016/j.dendro.2009.09.002>.
- Gat, J.R., 1996. Oxygen and Hydrogen Isotopes in the Hydrologic Cycle. *Annu. Rev. Earth Planet. Sci.* 24, 225–262. <https://doi.org/10.1146/annurev.earth.24.1.225>.
- Goldsmith, G.R., Allen, S.T., Braun, S., Engbersen, N., González-Quijano, C.R., Kirchner, J.W., Siegwolf, R.T.W., 2019. Spatial variation in throughfall, soil, and plant water isotopes in a temperate forest. *Ecology* 12. <https://doi.org/10.1002/eco.2059>.
- Gori, Y., Wehrens, R., Greule, M., Keppler, F., Ziller, L., La Porta, N., Camin, F., 2013. Carbon, hydrogen and oxygen stable isotope ratios of whole wood, cellulose and lignin methoxyl groups of *Picea abies* as climate proxies. *Rapid Commun. Mass Spectrom.* 27, 265–275. <https://doi.org/10.1002/rcm.6446>.
- Greule, M., Mosandl, A., Hamilton, J.T.G., Keppler, F., 2008. A rapid and precise method for determination of D/H ratios of plant methoxyl groups. *Rapid Commun. Mass Spectrom.* 22, 3983–3988. <https://doi.org/10.1002/rcm.3817>.
- Hartl-Meier, C., Zang, C., Büntgen, U., Esper, J., Rothe, A., Göttele, A., Dirnböck, T., Treydte, K., 2014. Uniform climate sensitivity in tree-ring stable isotopes across species and sites in a mid-latitude temperate forest. *Tree Physiol.* 35, 4–15. <https://doi.org/10.1093/treephys/tpu096>.
- Hilasvuori, E., Berninger, F., Sonninen, E., Tuomenvirta, H., Jungner, H., 2009. Stability of climate signal in carbon and oxygen isotope records and ring width from Scots pine (*Pinus sylvestris* L.) in Finland. *J. Quat. Sci.* 24, 469–480. <https://doi.org/10.1002/jqs.1260>.
- Holmes, R.L., 1983. Computer-assisted quality control in tree-ring dating and measurement. *Tree Ring Bull.* <https://doi.org/10.1016/j.ecoleng.2008.01.004>.
- Hsieh, J.C.C., Chadwick, O.A., Kelly, E.F., Savin, S.M., 1998. Oxygen isotopic composition of soil water: quantifying evaporation and transpiration. *Geoderma* 82, 269–293. [https://doi.org/10.1016/S0016-7061\(97\)00105-5](https://doi.org/10.1016/S0016-7061(97)00105-5).
- Hurrell, J.W., 1995. Decadal trends in the North Atlantic Oscillation: regional temperatures and precipitation. *Science* 269 (80), 676–679. <https://doi.org/10.1126/science.269.5224.676>.
- IAEA/WMO, 2020. *Global Network Of isotopes in Precipitation. (The GNIP Database)*.
- Jones, P.D., Jonsson, T., Wheeler, D., 1997. Extension to the North Atlantic oscillation using early instrumental pressure observations from Gibraltar and south-west Iceland. *Int. J. Climatol.* 17, 1433–1450. [https://doi.org/10.1002/\(sici\)1097-0088\(199711\)17:13<1433::aid-joc203>3.3.co;2-g](https://doi.org/10.1002/(sici)1097-0088(199711)17:13<1433::aid-joc203>3.3.co;2-g).
- Kanner, L.C., Buening, N.H., Stott, L.D., Timmermann, A., Noone, D., 2014. The role of soil processes in $\delta^{18}O$ terrestrial climate proxies. *Glob. Biogeochem. Cycles* 28, 239–252. <https://doi.org/10.1002/2013GB004742>.
- Keppler, F., Harper, D.B., Kalin, R.M., Meier-Augenstein, W., Farmer, N., Davis, S., Schmidt, H.-L., Brown, D.M., Hamilton, J.T.G., 2007. Stable hydrogen isotope ratios of lignin methoxyl groups as a paleoclimate proxy and constraint of the geographical origin of wood. *New Phytol.* 176, 600–609. <https://doi.org/10.1111/j.1469-8137.2007.02213.x>.
- Kraus, C., Zang, C., Menzel, A., 2016. Elevational response in leaf and xylem phenology reveals different prolongation of growing period of common beech and Norway spruce under warming conditions in the Bavarian Alps. *Eur. J. For. Res.* 135, 1011–1023. <https://doi.org/10.1007/s10342-016-0990-7>.
- Labuhn, I., Daux, V., Pierre, M., Stievenard, M., Girardclos, O., Féron, A., Genty, D., Masson-Delmotte, V., Mestre, O., 2014. Tree age, site and climate controls on tree ring cellulose $\delta^{18}O$: a case study on oak trees from south-western France. *Dendrochronologia* 32, 78–89. <https://doi.org/10.1016/j.dendro.2013.11.001>.
- Liu, X., An, W., Treydte, K., Wang, W., Xu, G., Zeng, X., Wu, G., Wang, B., Zhang, X., 2015. Pooled versus separate tree-ring δD measurements, and implications for reconstruction of the Arctic Oscillation in northwestern China. *Sci. Total Environ.* 511, 584–594. <https://doi.org/10.1016/j.scitotenv.2015.01.002>.
- Ljungqvist, F.C., Piermattei, A., Seim, A., Krusic, P.J., Büntgen, U., He, M., Kiryanov, A.V., Luterbacher, J., Schneider, L., Seftigen, K., Stahle, D.W., Villalba, R., Yang, B., Esper, J., 2020. Ranking of tree-ring based hydroclimate reconstructions of the past millennium. *Quat. Sci. Rev.* 230, 106074. <https://doi.org/10.1016/J.QUASCIREV.2019.106074>.
- McCarroll, D., Loader, N.J., 2004. Stable isotopes in tree rings. *Quat. Sci. Rev.* 23, 771–801. <https://doi.org/10.1016/j.quascirev.2003.06.017>.
- Michelot, A., Simard, S., Rathgeber, C., Dufréne, E., Damesin, C., 2012. Comparing the intra-annual wood formation of three European species (*Fagus sylvatica*, *Quercus petraea* and *Pinus sylvestris*) as related to leaf phenology and non-structural carbohydrate dynamics. *Tree Physiol.* 32, 1033–1045. <https://doi.org/10.1093/treephys/tps052>.
- Mischel, M., Esper, J., Keppler, F., Greule, M., Werner, W., 2015. $\delta^{2}H$, $\delta^{13}C$ and $\delta^{18}O$ from whole wood, α -cellulose and lignin methoxyl groups in *Pinus sylvestris*: a multi-parameter approach. *Isot. Environ. Health Stud.* 51, 553–568. <https://doi.org/10.1080/10256016.2015.1056181>.
- Morice, C.P., Kennedy, J.J., Rayner, N.A., Jones, P.D., 2012. Quantifying uncertainties in global and regional temperature change using an ensemble of observational estimates: the HadCRUT4 data set. *J. Geophys. Res. Atmos.* 117, 1–22. <https://doi.org/10.1029/2011JD017187>.
- Paul, D., Skrzypczak, G., Fórizs, I., 2007. Normalization of measured stable isotopic compositions to isotope reference scales – a review. *Rapid Commun. Mass Spectrom.* 21, 3006–3014. <https://doi.org/10.1002/rcm.3185>.
- Pauly, M., Helle, G., Miramont, C., Büntgen, U., Treydte, K., Reinig, F., Guibal, F., Sivan, O., Heinrich, I., Riedel, F., Kromer, B., Balanzategui, D., Wacker, L., Sookdeo, A., Brauer, A., 2018. Subfossil trees suggest enhanced Mediterranean hydroclimate variability at the onset of the Younger Dryas. *Sci. Rep.* 8, 1–8. <https://doi.org/10.1038/s41598-018-32251-2>.
- Riechelmann, D.F.C., Greule, M., Siegwolf, R.T.W., Anhäuser, T., Esper, J., Keppler, F., 2017. Warm season precipitation signal in δ^2H values of wood lignin methoxyl groups from high elevation larch trees in Switzerland. *Rapid Commun. Mass Spectrom.* 31, 1589–1598. <https://doi.org/10.1002/rcm.7938>.
- Roden, J.S., Ehleringer, J.R., 1999. Hydrogen and oxygen isotope ratios of tree-ring cellulose for riparian trees grown long-term under hydroponically controlled environments. *Oecologia* 121, 467–477. <https://doi.org/10.1007/s004420050953>.
- Roden, J.S., Lin, G., Ehleringer, J.R., 2000. A mechanistic model for interpretation of hydrogen and oxygen isotope ratios in tree-ring cellulose. *Geochim. Cosmochim. Acta* 64, 21–35. [https://doi.org/10.1016/S0016-7037\(99\)00195-7](https://doi.org/10.1016/S0016-7037(99)00195-7).
- Rozanski, K., Araguás-Araguás, L., Gonfiantini, R., 1993. Isotopic Patterns in Modern Global Precipitation. pp. 1–36. doi:<https://doi.org/10.1029/GM078p0001>.
- Schimmelmann, A., 1991. Determination of the concentration and stable isotopic composition of nonexchangeable hydrogen in organic matter. *Anal. Chem.* 63, 2456–2459. <https://doi.org/10.1021/ac00021a013>.
- Sodemann, H., Zubler, E., 2010. Seasonal and inter-annual variability of the moisture

- sources for alpine precipitation during 1995–2002. *Int. J. Climatol.* 30, 947–961. <https://doi.org/10.1002/joc.1932>.
- Sternberg, L. da S.L.O., 2009. Oxygen stable isotope ratios of tree-ring cellulose: the next phase of understanding. *New Phytol.* 181, 553–562. <https://doi.org/10.1111/j.1469-8137.2008.02661.x>.
- Szymczak, S., Joachimski, M.M., Bräuning, A., Hetzer, T., Kuhlemann, J., 2012. Are pooled tree ring $\delta^{13}\text{C}$ and $\delta^{18}\text{O}$ series reliable climate archives? - a case study of *Pinus nigra* spp. *laricio* (Corsica/France). *Chem. Geol.* 308–309, 40–49. <https://doi.org/10.1016/j.chemgeo.2012.03.013>.
- Tang, K., Feng, X., Ettl, G.J., 2000. The variations in δD of tree rings and the implications for climatic reconstruction. *Geochim. Cosmochim. Acta* 64, 1663–1673. [https://doi.org/10.1016/S0016-7037\(00\)00348-3](https://doi.org/10.1016/S0016-7037(00)00348-3).
- Treydte, K.S., Schleser, G.H., Helle, G., Frank, D.C., Winiger, M., Haug, G.H., Esper, J., 2006. The twentieth century was the wettest period in northern Pakistan over the past millennium. *Nature* 440, 1179–1182. <https://doi.org/10.1038/nature04743>.
- Voelker, S.L., Brooks, J.R., Meinzer, F.C., Roden, J., Voelker, S.L., Brooks, J.R., Meinzer, F.C., Roden, J., Pazdur, A., Pawelczyk, S., Hartsough, P., Snyder, K., Plavcova, L., Santrucek, J., 2014. Reconstructing relative humidity from plant $\delta^{18}\text{O}$ and δD as deuterium deviations from the global meteoric water line Published by: Wiley on behalf of the Ecological Society of America Stable URL: <http://www.jstor.org/stable/24432231> Reconstructing rela. *Ecol. Appl.* 25, 960–975.
- Waterhouse, J.S., Switsur, V.R., Barker, A.C., Carter, A.H.C., Robertson, I., 2002. Oxygen and hydrogen isotope ratios in tree rings: how well do models predict observed values? *Earth Planet. Sci. Lett.* 201, 421–430. [https://doi.org/10.1016/S0012-821X\(02\)00724-0](https://doi.org/10.1016/S0012-821X(02)00724-0).
- Wigley, T.M.L., Briffa, K.R., Jones, P.D., 1984. On the average value of correlated time series, with applications in dendroclimatology and hydrometeorology. *J. Clim. Appl. Meteorol.* 23, 201–213. [https://doi.org/10.1175/1520-0450\(1984\)023<0201:OTAVOC>2.0.CO;2](https://doi.org/10.1175/1520-0450(1984)023<0201:OTAVOC>2.0.CO;2).
- Wilson, A.T., Grinsted, M.J., 1977. $^{12}\text{C}/^{13}\text{C}$ in cellulose and lignin as palaeothermometers. *Nature* 265, 133–135. <https://doi.org/10.1038/265133a0>.
- Yapp, C.J., Epstein, S., 1982. A reexamination of cellulose carbon-bound hydrogen δD measurements and some factors affecting plant-water D/H relationships. *Geochim. Cosmochim. Acta* 46, 955–965. [https://doi.org/10.1016/0016-7037\(82\)90051-5](https://doi.org/10.1016/0016-7037(82)90051-5).
- Zweifel, R., Böhm, J.P., Häsler, R., 2002. Midday stomatal closure in Norway spruce - Reactions in the upper and lower crown. *Tree Physiol.* 1125–1136. <https://doi.org/10.1093/treephys/22.15-16.1125>.